iScience

CellPress
OPEN ACCESS

Article

Circadian Dysregulation of the TGFβ/SMAD4 Pathway Modulates Metastatic Properties and Cell Fate Decisions in Pancreatic Cancer Cells

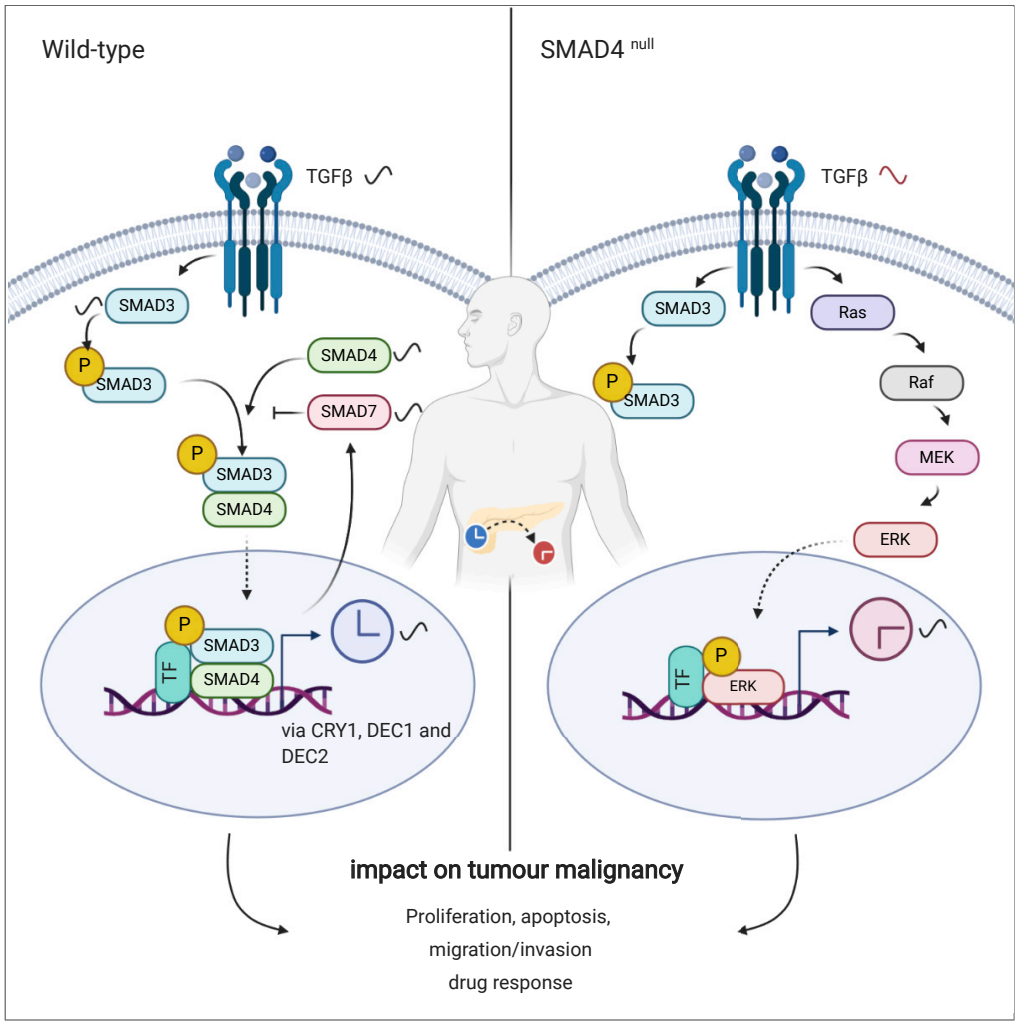

Yin Li, Alireza Basti, Müge Yalçin, Angela Relógio

angela.relogio@charite.de

HIGHLIGHTS

Transcripts of the canonical TGFβ pathway are rhythmically expressed in SMAD4$^{+/+}$ PDA

A reciprocal interplay exists between the TGFβ pathway and the circadian clock in SMAD4$^{+/+}$ PDA

SMAD4-WT and SMAD4-Null cells exibit differential circadian regulation of cell-fate decisions

Drug administration in PDA cells shows time- and SMAD4-dependent effects

Li et al., iScience *23*, 101551
October 23, 2020
https://doi.org/10.1016/j.isci.2020.101551

iScience

CellPress
OPEN ACCESS

Article

Circadian Dysregulation of the TGFβ/SMAD4 Pathway Modulates Metastatic Properties and Cell Fate Decisions in Pancreatic Cancer Cells

Yin Li,[1,2] Alireza Basti,[1,2] Müge Yalçin,[1,2] and Angela Relógio[1,2,3,4,*]

SUMMARY

Impairment of circadian rhythms impacts carcinogenesis. *SMAD4*, a clock-controlled gene and central component of the TGFβ canonical pathway, is frequently mutated in pancreatic ductal adenocarcinoma (PDA), leading to decreased survival. Here, we used an *in vitro* PDA model of SMAD4-positive and SMAD4-negative cells to investigate the interplay between circadian rhythms, the TGFβ canonical signaling pathway, and its impact on tumor malignancy. Our data show that *TGFβ1*, *SMAD3*, *SMAD4*, and *SMAD7* oscillate in a circadian fashion in SMAD4-positive PDA cells, whereas altering the clock impairs the mRNA dynamics of these genes. Furthermore, the expression of the clock genes *DEC1*, *DEC2*, and *CRY1* varied depending on SMAD4 status. TGFβ pathway activation resulted in an altered clock, cell-cycle arrest, accelerated apoptosis rate, enhanced invasiveness, and chemosensitivity. Our data suggest that the impact of TGFβ on the clock is SMAD4-dependent, and *SMAD3*, *SMAD4*, *DEC1*, and *CRY1* involved in this cross-talk affect PDA patient survival.

INTRODUCTION

In mammals, an internal biological timing system, the circadian clock coordinates the time of behavioral activities and physiological processes. At the molecular level, the circadian clock is composed of a set of genes and their protein products, interconnected by transcriptional/translational feedback loops (Fuhr et al., 2015). This core-clock network (CCN) generates endogenous 24-h oscillations in the expression of genes and proteins and is involved in the circadian regulation of various cellular processes, including the cell cycle (El-Athman et al., 2017), apoptosis (Gery et al., 2005; Wang et al., 2016), DNA repair (Di Micco et al., 2011), the epithelial-to-mesenchymal transition (EMT) (Mao et al., 2012), metabolism (Fuhr et al., 2018; Reinke and Asher, 2019), and immunity (Abreu et al., 2018). Its aberrant function impacts cell functioning and can lead to the development and progression of several diseases including cancer (Davis et al., 2019; Sulli et al., 2019; Yalcin et al., 2020). Genes involved in cell cycle regulation (e.g., *MYC*, *WEE1*, and *INK4A*), immune function (e.g., *TNF*), and metabolism (e.g., *SIRT3*, *CPT1*, and *PDH*) show a rhythmic pattern of expression and are known clock-controlled genes (CCGs).

The transforming growth factor β (TGFβ) transduction pathway is among the clock-controlled pathways involved in oncogenic transformation. The TGFβ pathway is implicated in the maintenance of tissue homeostasis, regulation of fetal development, immune system control, wound repair, and EMT (Massague, 2008). The basic elements of the canonical TGFβ pathway include TGFβ cytokines, receptors, and Smads (Smad4, receptor-Smads, and inhibitory-Smads). TGFβ activates downstream pathways by binding to two pairs of receptors (type I and type II receptors). Once the receptors are activated, reporter-Smads (R-Smads) undergo phosphorylation, which results in signal propagation. The activated R-Smads (Smad2 and Smad3) translocate to the nucleus and form a complex with Smad4. Activated Smad complexes regulate gene expression by DNA-binding activity, and inhibitory-Smads (Smad7) prevent this complex formation (Massague, 2008; Prunier et al., 2019).

In normal and premalignant cells, TGFβ functions as tumor suppressor via the regulation of cytostasis, differentiation, cell cycle, apoptosis, and suppression of inflammation, and malfunctions in the TGFβ signaling pathway can result in tumorigenesis (Cheng et al., 2001; Massague, 2008; Principe et al., 2017; Scandura et al., 2004; Siegel and Massague, 2003).

[1]Charité - Universitätsmedizin Berlin, Corporate Member of Freie Universität Berlin, Humboldt - Universität zu Berlin, and Berlin Institute of Health, Institute for Theoretical Biology, Berlin, Germany

[2]Charité - Universitätsmedizin Berlin, Corporate Member of Freie Universität Berlin, Humboldt - Universität zu Berlin, and Berlin Institute of Health, Medical Department of Hematology, Oncology, and Tumour Immunology, Molecular Cancer Research Centre, Berlin, Germany

[3]MSH Medical School Hamburg GmbH–University of Applied Sciences and Medical University, Department of Human Medicine, Institute for Systems Medicine and Bioinformatics, Hamburg, Germany

[4]Lead Contact

*Correspondence: angela.relogio@charite.de

https://doi.org/10.1016/j.isci.2020.101551

Pancreatic ductal adenocarcinoma (PDA) is a malignant disease with poor prognosis and low overall survival rate, and it is the fourth leading cause of cancer death in the European Union and the United States (Coveler et al., 2016). More than half of the patients with PDA harbor mutations in *SMAD4*. The inactivation of *SMAD4* in tumors is a common event in advanced-stage PDA and is linked to poorer prognosis (Singh et al., 2012).

Interestingly, several components of the TGFβ canonical pathway are circadian regulated in different organisms (Akagi et al., 2017; Chen et al., 2015; Sato et al., 2019). Previous studies reported circadian expression of TGFβ1 and Smad3 (transcripts or proteins) in mouse brown adipocyte (Nam et al., 2015), mouse kidney (Sato et al., 2019), and mouse heart (Sato et al., 2017). In addition, the oscillating pattern *of TGFβ1* was altered after the disruption of *Clock* (Chen et al., 2015). However, it remains unclear whether components of the TGFβ canonical signaling (including *TGFβ1*, *SMAD4*, *SMAD3,* and *SMAD7*) are clock regulated in human cancer cells and whether circadian disruption affects these elements in cancer cells with consequences on tumor malignancy. Work from our group indicates that *Smad4*, the core mediator of the TGFβ canonical pathway, is regulated indirectly by the circadian clock (Lehmann et al., 2015). Wu et al. reported the binding of Smad3 or Smad4 to the Smad-binding elements in the *DEC1* promoter in pancreatic cancer cells, further contributing to their circadian regulation (Wu et al., 2012). These studies pointed to a link bridging the circadian and TGFβ pathway.

Despite current findings regarding rhythmicity in elements of the TGFβ pathway and the functionality of this pathway, the reciprocal interplay between the TGFβ/SMAD4 pathway, the circadian clock, and its impact on tumor progression remains unclear in PDA.

Here, we investigated the influence of a dysregulated biological clock on PDA progression using an *in vitro* cellular model system. For this, we used SMAD4 wild-type and mutant PDA cell lines, derived respectively, from the primary tumor and the metastatic lesions of patients with PDA. We further explored the impact of clock dysregulation on the TGFβ/SMAD4 canonical pathway. Our results show that elements of the TGFβ canonical pathway (including *SMAD3*, *SMAD4*, *SMAD7,* and *TGFβ1*) are expressed in a circadian manner in SMAD4 wild-type PDA cells. In addition, we found that the rhythmic expression of the above-mentioned transcripts was altered upon the dysregulation of the circadian clock, suggesting that these TGFβ canonical elements are under circadian modulation. Our data point to a modulation of the TGFβ canonical pathway via the clock through interactions with the transcription factors *DEC1*, *DEC2,* and the core-clock gene *CRY1*. Also, we explored the influence of the canonical TGFβ pathway on the clock phenotype in these cells. Our results indicated that the activation of the TGFβ canonical pathway through *SMAD4* overexpression and TGFβ induction results in a faster clock in PDA cells. Also, genetic modifications of *SMAD4* (knockdown or overexpression) altered the expression of the core-clock genes *BMAL1*, *PER2*, *NR1D1,* and *CRY1*, and of the clock- and TGFβ-controlled genes, *DEC1* and *DEC2*.

Furthermore, we investigated proliferation, apoptosis, migration, and invasion in clock-disrupted (*shBMAL1*, *shPER2,* and *shNR1D1* knockdown) and *SMAD4* up- or downregulated PDA cells, as well as the effects of a dysregulated clock on drug sensitivity in both SMAD4-proficient and SMAD4-deficient PDA cell lines. Our data provide evidence for *SMAD4*- and clock-dependent drug response in PDA cells, and highlight the role of the bidirectional interaction between the biological clock and the TGFβ/SMAD4 canonical pathway in cell cycle, apoptosis, and cancer metastasis in pancreatic cancer cells, which may further affect patient survival.

RESULTS

Bidirectional Interplay between the Circadian Clock and TGFβ Canonical Pathway

To investigate the impact of a dysregulated clock in cancer metastasis and cell fate decisions in a pancreatic cancer cellular model, we used an established *in vitro* model of SMAD4-proficient (Panc1) and SMAD4-deficient (AsPC1) pancreatic adenocarcinoma cells (PDA), derived from different anatomical patient lesions (primary tumor and metastasis ascites, respectively) representing PDA tumors at different stages. Panc1 (ATCC: CRL-1469) is derived from the primary tumor of a male patient. The cell line AsPC1 (ATCC: CRL-1682) was established from ascites of a female patient with PDA. The doubling time of both cell lines is very similar and close to 52 h (Lieber et al., 1975; Watanabe et al., 2012). In addition, we analyzed cell growth of wild-type Panc1 and AsPC1 in our work using cell nucleus fluorescence labeling, which shows similar growth curves within 72 h for both cell lines (n ± SEM, n = 8, Figure S1D). Hence, both cell lines show similar cell cycle dynamics, making them suitable for our study. Of note, both cell lines carry mutated forms of *KRAS*, *p16,* and *TP53* (Berrozpe et al., 1994; Kita et al., 1999; Sun et al., 2001). Furthermore, our preliminary

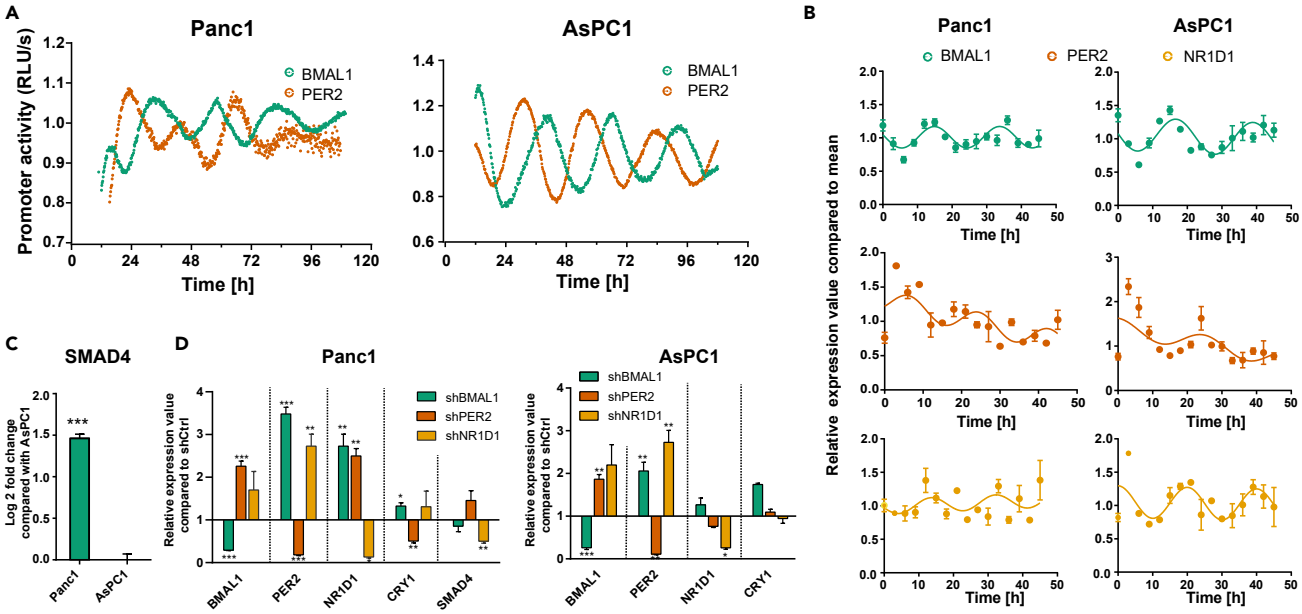

Figure 1. Panc1 and AsPC1 Cell Lines Harbor Different Clock Phenotypes

(A) Panc1 and AsPC1 cells were lentivirally transduced with a *BMAL1* promoter (green) or *PER2* promoter (orange)-driven luciferase construct. Bioluminescence was measured for 5 consecutive days. Depicted is one representative replicate for each condition.

(B) The 48 h time course RT-qPCR measurements of selected core-clock genes (*BMAL1*, *PER2*, and *NR1D1*) in Panc1 and AsPC1 WT cells.

(C) The relative mRNA levels of *SMAD4* compared with AsPC1.

(D) RT-qPCR measurements after knockdown of core-clock genes (*shBMAL1*, *shPER2*, and *shNR1D1*) in Panc1 and AsPC1 cells.

Data are expressed as mean ± SEM, n = 3, *p < 0.05, **p < 0.01, ***p < 0.001. See also Figures S1 and S2.

work for this study (via computational network analysis) showed that, among the highly mutated genes in PDA (above 5% mutation rate), SMAD4 is tightly correlated with the CCN and has an impact on patient outcome (Cancer Genome Atlas Research Network, 2017; Lehmann et al., 2015).

Both cell lines showed oscillations, but with smaller amplitudes and shorter period for the Panc1 cells (*BMAL1*: 26.1 ± 0.3 h, n = 3) when compared with the AsPC1 cells (*BMAL1*: 27.4 ± 0.6 h, n = 3, Figure 1A). The oscillation parameters of PER2:Luc are provided in Table 1. We performed a 48 h time course RT-qPCR analysis, which confirmed the phenotypes observed in our luminescence data for *BMAL1* and *PER2* with an anti-phasic oscillation in both PDA cells (Figures 1A and 1B, Tables 1 and 2). Thus, according to our data, the endogenous time machinery operates differentially in these PDA cell lines.

Next, to explore the impact of clock disruption in the TGFβ pathway, we produced knockdown PDA cell lines for the core-clock genes *BMAL1*, *PER2*, and *NR1D1* and evaluated the output in terms of gene expression (Figures 1D, S1B, and S1C). *SMAD4* expression in Panc1 cells was significantly higher when compared with that of AsPC1 (Figure 1C, ***p < 0.001). We confirmed that AsPC1 is a SMAD4-deficient cell line at the protein level (Figure S1A), as previously reported (Schutte et al., 1996; Sun et al., 2001). Furthermore, *SMAD4* expression was downregulated in Panc1-*shBMAL1* and Panc1-*shNR1D1* cells at 3 h after cell synchronization (Figure 1D, Panc1, **p < 0.01, n = 3). Interestingly, the downregulation of *BMAL1* and *NR1D1* impacts the rhythmic expression of *SMAD4* in the SMAD4-proficient PDA cells (Figure 2A).

We further evaluated the consequences of these perturbations on the clock phenotype (Figure S2). The downregulation of *BMAL1* and *PER2* in Panc1 cells resulted in an almost complete loss of oscillations, whereas *NR1D1* KD (knockdown) showed no significant effect on the rhythmicity of *BMAL1*. The downregulation of *BMAL1* in AsPC1 cells led to a complete loss of oscillations, and AsPC1-*shNR1D1* cells depicted a significant shorter period.

Our results point to a connection between core-clock elements and *SMAD4*. To further investigate this interplay, we quantified the expression of *SMAD3*, *SMAD4*, *SMAD7*, and *TGFβ1* in our *in vitro* model (Figure S3).

	Panc1	AsPC1
Period (h)	26.6 ± 2.7	26.4 ± 0.4
Phase (h)	22.1 ± 2.7	5.2 ± 0.5
Amplitude	0.2 ± 0.0	0.2 ± 0.1
CC	0.9 ± 0.1	0.9 ± 0.1
Phase shift relative to BMAL1 (h)	15.0	6.8

Table 1. Circadian Parameters of *PER2* Promoter Activity in PDA Cells (Chronostar Analysis)

According to previous studies in other model systems (Chen et al., 2015; Nam et al., 2015), Clock-Bmal1 heterodimers or Bmal1 activate the expression of *Tgfβ*, *Smad3* by binding to their promoter regions. Particularly, the robust circadian rhythmicity of *mTgfβ1* is abolished in *mClock*-KO mice (Chen et al., 2015). Such findings suggest the existence of a circadian regulation of these TGFβ signaling components at the transcriptome level. Thereby, we hypothesized that this phenomenon might also exist in human PDA cancer cells. We found rhythmic expression of *TGFβ1* in both the SMAD4-proficient and SMAD4-deficient PDA cells (Figures S3A and S3E). Surprisingly, we also observed circadian oscillations in the expression of *SMAD3*, *SMAD4,* and *SMAD7* in SMAD4 WT cells (Panc1, Figures S3B–S3D and Table 3). Interestingly, *SMAD3* and *TGFβ1* transcripts oscillated with slightly different phases and similar periods as *BMAL1* in SMAD4-proficient cells (Panc1, Figure S3, Tables 2 and 3). However, the oscillation of *TGFβ1* exhibited longer periods (~27 h) when compared with *BMAL1* (22.3 ± 0.9 h) in SMAD4-deficient cells (AsPC1, Figure S3E), implying that the correlation between the rhythmic expression of *TGFβ1* and *BMAL1* is likely SMAD4 dependent. Furthermore, we compared the expression level of these components for the PDA cell lines in a 39 h time course (Figures S3F–S3H). The mRNA levels of *SMAD3* and *SMAD7* (Figures S3G and S3H) were much reduced in AsPC1 when compared with Panc1, whereas *TGFβ1* was highly expressed in AsPC1 when compared with Panc1 (Figure S3F). These data point to the inactivation of the TGFβ canonical pathway in SMAD4-deficient PDA cells, which may result in altered interaction with the clock machinery and ultimately support further progression towards malignant phenotypes.

We further explored the reciprocal interplay between the core-clock and the TGFβ canonical pathway and analyzed the effect of perturbing the core-clock elements on the expression of several components of the TGFβ canonical pathway (*SMAD3*, *SMAD7,* and *TGFβ1*).

A former study suggested *Bmal1* and *Nr1d1* to be key clock elements bridging the clock and the TGFβ canonical pathway in mouse adipocytes (Nam et al., 2015). Hence, we performed a 24 h time course RT-qPCR for *BMAL1* and *NR1D1* KDs and *shCtrl* in Panc1 cells. The expression of *TGFβ1*, *SMAD3*, *SMAD4,* and *SMAD7* exhibited a large variation after the *BMAL1* and *NR1D1* KDs when compared with *shCtrl* (Figure 2A). In particular, in Panc1-*shBMAL1* and Panc1-*shNR1D1* cells, the expression of *SMAD4* reached its peak at 18 h after synchronization. As previously reported, Bmal1 binding to the promoter region of *Smad3* (resulting in activation of *Smad3*) occurred at a specific time point (CT8 in mice) (Nam et al., 2015). Our results show that clock dysregulation (*BMAL1* KD) repressed *SMAD3* and *SMAD7* transcripts at 21 h after synchronization, suggesting that the inactivation of the TGFβ canonical pathway (particularly *SMAD7* as an indicator of the TGFβ pathway activation) occurs at a specific time point after the clock disruption (Figure 2A). The *TGFβ1* transcript was overexpressed upon *BMAL1* KD over the time of the measurements (Figure 2A). These data indicated that the disruption of *BMAL1* and *NR1D1* modified the time-dependent variations of elements of the TGFβ pathway (Figures 2A and S3). We observed a similar expression pattern of *SMAD3* and *SMAD7* upon *BMAL1* and *NR1D1* KDs, indicating that these elements may assist to set up a rapid reciprocal cross-talk between the TGFβ canonical pathway and the circadian clock (Figure 2A).

We then measured *BMAL1*- and *PER2*-promoter activity in *SMAD4*-KD and overexpression (*SMAD4*-OE) cells when compared with the corresponding control conditions (*shCtrl* or oeCtrl) and with additional TGFβ1 stimulation, to explore the impact of the TGFβ pathway on the clock phenotype. Overexpression efficiency was analyzed at the transcript and protein levels (Figure S5A and S5B). The activation of the TGFβ canonical pathway by *SMAD4*-OE and additional TGFβ1 stimulation significantly shortened the period of the oscillations (Figures 2E, 2F, 2H, 2I, and S4A–S4C, *$p < 0.05$, $n = 3$). In addition, *SMAD4*-KD

Cosinor Analysis			
	Panc1		
	BMAL1	PER2	NR1D1
Phase (h)	17.0 ± 0.5	4.1 ± 0.7	14.4 ± 0.5
Period (h)	19.0 ± 1.0	18.3 ± 1.5	18.6 ± 0
Amplitude	0.2 ± 0.1	0.2 ± 0.1	0.1 ± 0.1
p Value	<0.0001	<0.0001	0.045
	AsPC1		
	BMAL1	PER2	NR1D1
Phase (h)	14.4 ± 0.3	0 ± 3.6	20 ± 0.0
Period (h)	22.3. ± 0.9	24.8 ± 0.0	20.0 ± 1.3
Amplitude	0.3 ± 0.0	0.2 ± 0.1	0.2 ± 0.1
p Value	<0.0001	<0.0001	0.0003

Table 2. Circadian Parameters Retrieved with Cosinor Analysis for a 48 h Time Course RT-qPCR Data (*BMAL1*, *PER2*, and *NR1D1*).

in Panc1 led to a shorter period when compared with *shCtrl* (Figures 2B and 2C, **p < 0.01), pointing to a putative role of *SMAD4* in the regulation of the circadian clock via *BMAL1*.

In addition, we evaluated the impact of *SMAD4* in the regulation of core-clock elements *BMAL1*, *PER2*, *NR1D1*, and *CRY1* and further analyzed the expression of the clock genes *DEC1* and *DEC2* (Figures 2D, 2G, and 2J), reported as mediators in the above cross-talk (Kon et al., 2008; Sato et al., 2016, 2019). Interestingly, most of the core-clock genes showed significant alterations for Panc1 *SMAD4*-OE and *SMAD4*-KD (Figures 2D and 2G). Overall, *CRY1* was upregulated, whereas *DEC1* and *DEC2* were downregulated in *SMAD4*-OE PDA cells (Figures 2D and 2J, *p < 0.05, **p < 0.01, ***p < 0.001, n = 3). In agreement, we observed the opposite results in Panc1-*shSMAD4* (Figure 2G, **p < 0.01, ***p < 0.001, n = 3). These results further reinforce the existence of a bidirectional connection between the core-clock and the SMAD4-dependent pathways via the regulation of *CRY1*, *DEC1*, and DEC2.

Dysregulation of the Core-Clock Genes *BMAL1*, *PER2*, and *NR1D1*, and Perturbations in *SMAD4* Impact Cell Proliferation and Apoptosis in PDA Cells

We further evaluated the effects of disrupting core-clock genes and *SMAD4* in cell fate decisions by analyzing cell proliferation and apoptosis. Interestingly, SMAD4-proficient (Panc1) and SMAD4-deficient (AsPC1) cells showed different effects on proliferation upon the different knockdowns (Figure 3A). Proliferation increased in Panc1 cells after *BMAL1* and *NR1D1* KDs, whereas this was not observed in AsPC1 knockdown cells (Figure 3A). Panc1-*shSMAD4* cells showed increased proliferation when compared with the *shCtrl*. However, *SMAD4*-OE in both PDA cells showed no significant difference in the proliferative ability compared with oeCtrl. These results indicate that the non-canonical pathway (which includes RAS, MAPK, JNK) might be activated after *SMAD4* KD, leading to an increase in proliferation. To verify our assumption, we measured RAS and phosphorylated-ERK (p-ERK) proteins in Panc1-*shCtrl* and Panc1-*shSMAD4* cells with and without a 24-h TGFβ1 stimulation. Our results show that the TGFβ1 stimulation activates the phosphorylation of ERK for both Panc1-*shCrtl* and Panc1-*shSMAD4* (Figures S6A and S6C). In addition, *SMAD4*-KD (particularly stimulated with TGFβ1) indeed upregulated the expression of RAS and p-ERK, when compared with control cells (Figures S6A–S6C). These data suggest the activation of the Ras pathway after the downregulation of SMAD4. In addition, the apoptotic profiles of PDA cells were altered upon core-clock dysregulation. The downregulation of *BMAL1*, *PER2*, and *NR1D1* increased apoptosis when compared with *shCtrl* (Figures 3B, 3C, and 3E). *SMAD4* OE promoted apoptosis in both PDA cells (Figures 3B, 3D, and 3F). These results implied that the upregulation of *SMAD4* and the disruption of core-clock genes induces apoptosis in our *vitro* model.

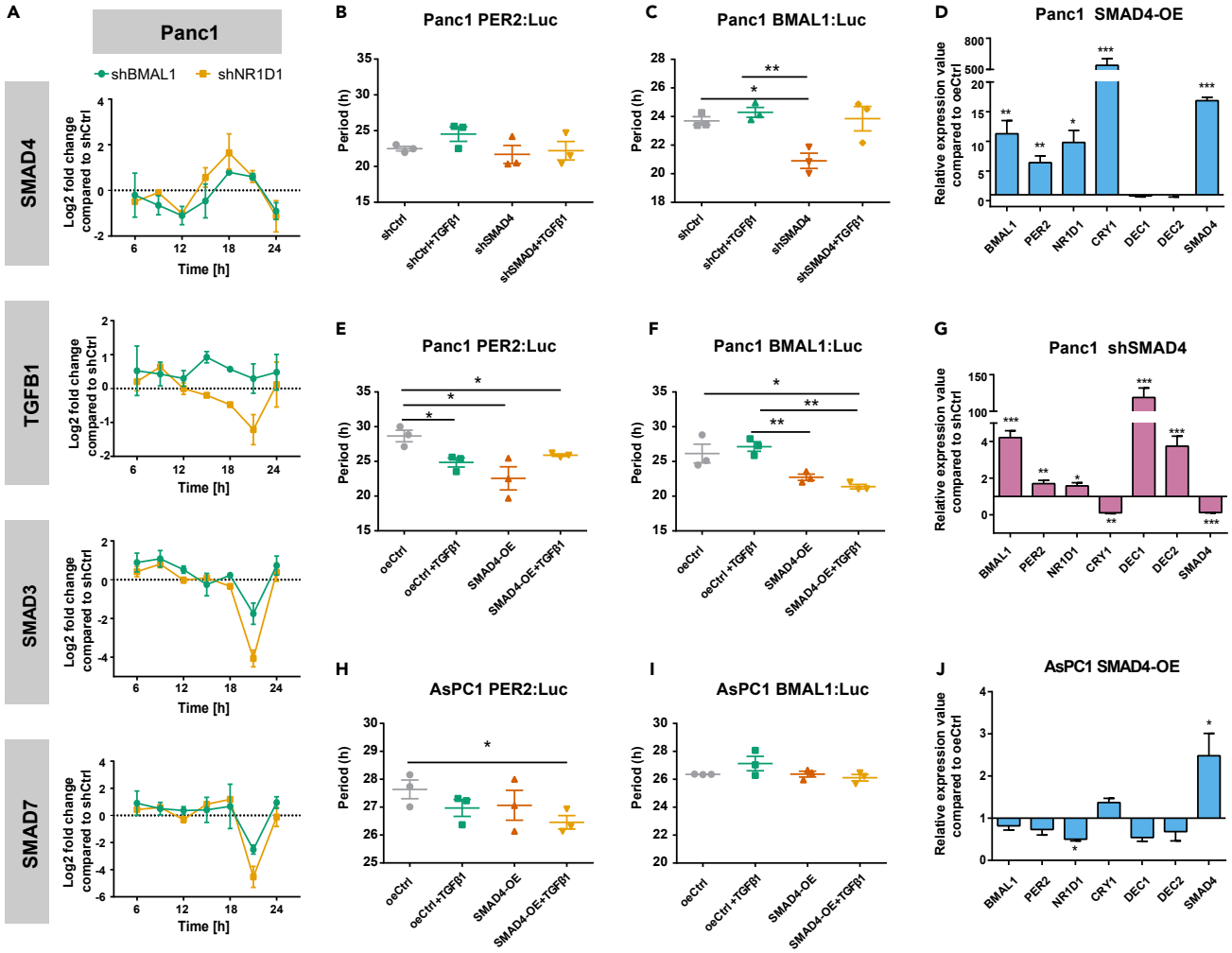

Figure 2. Panc1 and AsPC1 Cells as a Model for Investigating the Cross-Talk between the Circadian Clock and the TGFβ Canonical Pathway

(A) The 24 h time course RT-qPCR was carried out in Panc1 cells (A) containing *shCtrl* empty vector, *shBMAL1*, and *shNR1D1* constructs. Relative expression value of TGFβ signaling-associated genes (*SMAD4*, *TGFβ1*, *SMAD3*, and *SMAD7*) is shown compared with *shCtrl* cells at each time point.

(B, C, E, F, H, and I) *SMAD4*-KD or *SMAD4*-OE cells were lentivirally transduced with a *BMAL1*- or a *PER2*-promoter-driven luciferase construct. Bioluminescence was measured for 5 consecutive days with TGFβ1 or corresponding empty vehicle (0.1% BSA). Depicted are the periods for Panc1 (B, C, E, and F) and for AsPC1 (H and I) of *BMAL1* or *PER2* promoter activities, as indicated. One representative replicate for each condition is provided in Figure S4.

(D, G, and J) Effect of *SMAD4*-KD or *SMAD4*-OE on the expression of clock genes in Panc1 (D and G) and AsPC1 (J) cells.

Data are expressed as mean ± SEM, n = 3, one-way ANOVA (B, C, E, F, H, and I) or multiple t test (D, G, and J); *p < 0.05, **p < 0.01, ***p < 0.001. See also Figures S3, S4, and S5A–S5B.

Clock Dysregulation and the Activation of the TGFβ/SMAD4 Pathway Impacts Apoptosis and Cell Cycle in PDA Cells

To further characterize the putative effects of dysregulating the TGFβ/SMAD4 signal transduction in our model, we stimulated the pathway with TGFβ1 in addition to *SMAD4*-KD or *SMAD4*-OE and analyzed cell proliferation and apoptosis. The activation of the pathway (*SMAD4*-OE with TGFβ1 stimulation) did not alter proliferation in Panc1 cells, and its inactivation (*SMAD4*-KD with or without TGFβ1) promoted proliferation (Figures 4A and 4B). Interestingly, we observed increased proliferation in SMAD4-deficient cells (AsPC1) with TGFβ1 stimulations compared with *SMAD4*-OE cells (Figure 4C). Thus, we hypothesized that TGFβ1 triggers the downstream elements of the TGFβ non-canonical signaling pathway (e.g., RAS, PI3K) leading to increased proliferation in SMAD4-deficient cells.

The stimulation of TGFβ1 induced apoptosis particularly in SMAD4-positive PDA cells (including *SMAD4*-OE and wild-type, Figures 4E–4G).

Cosinor Analysis				
	Panc1			
	TGFβ1	SMAD3	SMAD7	SMAD4
Phase (h)	1.7 ± 1.5	19.1 ± 0.8	11.85 ± 1.3	12.6 ± 1.1
Period (h)	20.0 ± 3.8	21.8 ± 2.6	22.8 ± 4.7	21.7 ± 3.4
Amplitude	0.1 ± 0.1	0.3 ± 0.1	0.2 ± 0.1	0.3 ± 0.2
p Value	0.0015	0.0004	0.0001	0.0256
				AsPC1
				TGFβ1
Phase (h)				4.6 ± 0.3
Period (h)				27.0
Amplitude				0.2 ± 0.0
p Value				<0.0001

Table 3. Circadian Parameters Retrieved with Cosinor Analysis for a 33 h Time Course RT-qPCR Data (*TGFβ1, SMAD3, SMAD4,* and SMAD7).

We analyzed the cell cycle of the PDA cells in greater detail in all the aforementioned conditions. Our analysis showed significant cell-type-specific alterations upon KD of clock genes when compared with control cells. For the SMAD4-proficient cell line (Panc1), the percentage of cells in S phase decreased significantly and G2/M phase increased after *PER2* KD (Figure 4I, $^{**}p < 0.01$, $^{***}p < 0.001$, n = 3), whereas the percentage of cells in S phase increased after *NR1D1*, in agreement with the proliferation results. In AsPC1 cells, we observed a significant increase of S phase and decrease of G1 phase in *PER2* KD cells (Figure 4K, $^{**}p < 0.01$, $^{***}p < 0.001$, n = 3), and no significant alterations upon the KD of *BMAL1* and *NR1D1*, in agreement with our proliferation results (Figure 3A). The differential phenotypes observed might result from the different genomic background of both cell lines (in particular the *SMAD4* alteration) that subsequently impacts the circadian pathway, leading to an overall differential proliferative phenotype.

Next, we investigated the impact of TGFβ on the cell cycle. Panc1 cells depicted increased G1/S arrest upon TGFβ1 stimulation (Figures 4D and S5C). Interestingly, unlike the impact of TGFβ1 that has been reported in previous studies for other model systems (Alexandrow and Moses, 1995; Mukherjee et al., 2010), and also found in SMAD4-proficient cells, a 24-h TGFβ1 stimulation increased the percentage of cells in G2/M phase in *shNR1D1* cells (Figure S5C), pointing towards differential regulation of the cell cycle by TGFβ upon *NR1D1* downregulation. Additional TGFβ1 did not cause G1/S arrest in SMAD4-deficient cells (AsPC1, Figures 4H and S5D); this is distinct from the observations in SMAD4-proficient cells (Panc1) Instead, we observed an increase in G2/M or S phase in all KD conditions (*shBMAL1*, *shPER2,* and *shNR1D1*) and *shCtrl* cells upon TGFβ stimulation when compared with non-stimulated cells (Figures 4H and S5D). These results point to a SMAD4 dependency regarding the effects of TGFβ on cell cycle distribution. We further analyzed the cell cycle in *SMAD4*-KD and *SMAD4*-OE conditions with or without additional TGFβ1 stimulation (Figures 4I–4K). For Panc1, the additional TGFβ1 and upregulation of *SMAD4* led to increased number of cells in G1/S phase (Figures 4I and 4J). However, the impairment of the TGFβ canonical pathway (*SMAD4* KD) increased the number of cells in S phase particularly when compared with the activation of TGFβ canonical pathway (*shCtrl* with TGFβ1): G1 decreased and S phase increased (Figure 4J). In SMAD4-deficient cells (AsPC1), *SMAD4* OE with additional TGFβ1 stimulation resulted in an increased G1 and decreased S phase when compared with oeCtrl cells (Figure 4K). However, in AsPC1 oeCtrl cells, TGFβ1 stimulation led to an increase in the percentage of cells in S phase (Figure 4K) and consistently a higher proliferative potential (Figure 4C) when compared to non-stimulation oeCtrl. This finding further supports the activation of the non-canonical TGFβ pathway in the absence of SMAD4, which triggers the activation of the oncogene RAS (Figure S6) in the downstream pathway and subsequently affects cell cycle and proliferation.

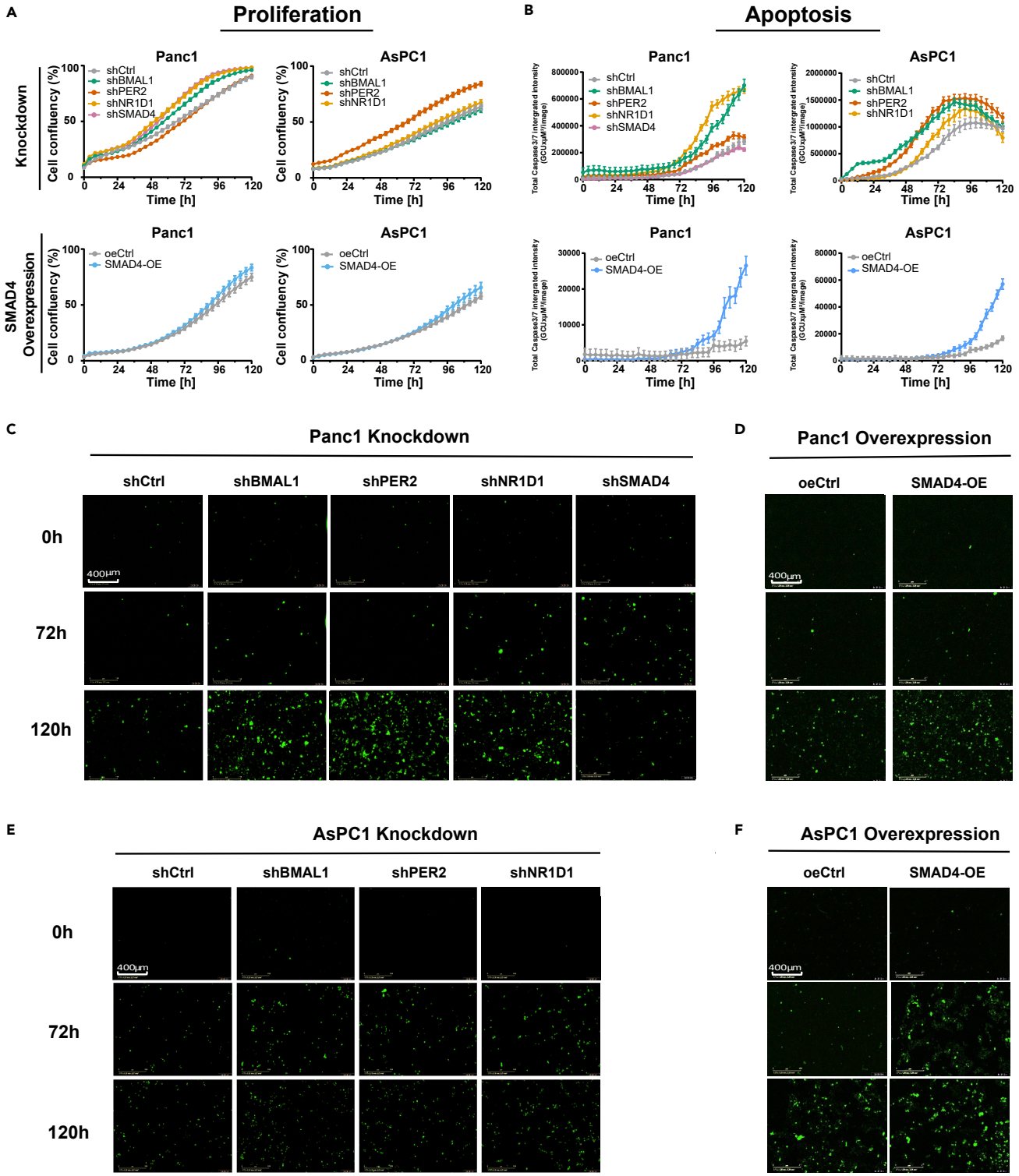

Figure 3. Dysregulation of the Core-Clock Genes (*BMAL1*, *PER2*, and *NR1D1*) and *SMAD4* Leads to Differential Cell Proliferation and Apoptosis in Panc1 and AsPC1 Cells

(A) Proliferation analyses of PDA cell lines for KD conditions (*shBMAL1*, *shPER2*, *shNR1D1*, and *shSMAD4*), *SMAD4*-OEs, and corresponding empty vectors (*shCtrl* and oeCtrl, respectively).

Figure 3. *Continued*

(B) Apoptosis analysis of PDA cell lines after KDs or OEs. Data are expressed as mean ± SEM, n ≥ 6 (A and B).

(C–F) Representative images of apoptosis assays for Panc1 *shCtrl* and knockdown cells *shBMAL1, shPER2, shNR1D1, shSMAD4* (C) or Panc1 oeCtrl and *SMAD4*-OE cells (D) and AsPC1 *shCtrl* and knockdown cells *shBMAL1, shPER2, shNR1D1* (E) or AsPC1 oeCtrl and *SMAD4*-OE cells (F), with fluorescently labeled caspase3/7 with (objective 20×) at time points 0, 72, and 120 h, respectively. Data are expressed as mean ± SEM, n ≥ 6 (A and B).

These results demonstrate that TGFβ canonical and non-canonical pathways regulate the cell cycle, proliferation, and apoptosis in a SMAD4-dependent manner.

The Dysregulation of the Core Clock Impacts Cell Migration in a SMAD4-Dependent Manner

Next, we aimed to examine if the activation of TGFβ/SMAD4 pathway may contribute to the formation of tumor metastasis. We used a real-time cell recording approach to measure the invasive and migration properties of these PDA cells, analyzed known EMT markers, and investigated morphological cellular alterations (Figure 5). TGFβ1 stimulation significantly increased the migration speed in both PDA cells, particularly in *SMAD4*-OE cells (Figures 5B, 5C, 5E, and 5F, *p < 0.05, ***p < 0.001, n = 8). For AsPC1 oeCtrl cells, TGFβ1 stimulation did not significantly promote migration likely due to its intrinsic *SMAD4* deficiency. In contrast, Panc1 cells showed a significantly slower migration speed after *SMAD4* KD (Figure 5D, **p < 0.01, n = 8) and TGFβ stimulation was not able to induce the migrative potential in *SMAD4* KD cells (Figures 5A and 5D), in agreement with previous data by Takano and colleagues who reported a role for SMAD4 in the expression of EMT marker genes in pancreatic cancer (Takano et al., 2007). In addition, the resembled phenomenon was found in invasion assays as well; TGFβ1 stimulation or *SMAD4* overexpression promoted the invasiveness of PDA cells (Figures 5H and 5I), whereas *SMAD4*-KD without additional TGFβ1 impaired invasive ability (Figure 5G). Altogether, these data suggest that the presence of intrinsic SMAD4 and TGFβ in the tumor microenvironment is crucial for tumor invasiveness and cell motility. Cells that undergo EMT have a greater tendency to invade and metastasize (Yang et al., 2020), thus we verified our results by quantifying EMT biological makers and examining alterations in cell morphology. The cadherins are major adhesion molecules anchoring in the cytomembrane. Epithelial cells express E-cadherin, whereas cells that show mesenchymal features express N-cadherin and R-cadherin (Wheelock et al., 2008). Cancer cells can enhance or reduce their metastatic potential through cadherin switching, which is one characteristic of the EMT. Also Vimentin, a cytoskeletal molecule responsible for maintaining cell integrity and resistance against stress (Satelli and Li, 2011), has been described as an EMT biomarker. Additionally, we also analyzed the transcription factors *SNAIL* and *SLUG* that are sensitive to microenvironmental stimuli and function as EMT switchers (Lamouille et al., 2014).

CD133 has been commonly used as an important biomarker to identify cancer stem cells (Glumac and LeBeau, 2018). We found a significant overexpression of *CD133* and *E-cadherin* and a downregulation of *Vimentin* and *SLUG* in Panc1 *SMAD4*-KD cells (Figure 5J, **p < 0.01, ***p < 0.001, n = 3). In contrast, *E-cadherin* expression decreased, whereas *N-cadherin, Vimentin, SNAIL,* and *SLUG* were significantly increased in both PDA cells after *SMAD4*-OE (Figures 5K and 5L, *p < 0.05, **p < 0.01, ***p < 0.001, n = 3), pointing to the initiation of the EMT process and gain of motility in *SMAD4*-OE cells, increasing the invasiveness potential of these cells. Furthermore, the decrease in the expression level of *CD133* after *SMAD4*-OE indicated a reduction of CSCs (cancer stemness cells) along with the increased levels of *SMAD4*. Interestingly, we observed morphological changes in the cells (from cuboidal shaped to spindle shaped), after the activation of the TGFβ canonical pathway (Figure S7). The morphological cellular change may facilitate cells to traverse the cellular matrix into intercellular spaces. Consistently, the upregulation of *Vimentin* pointed to an alteration of the cytoskeleton in *SMAD4*-OE cells (Figures 5K and 5L). However, this morphological change was not observed in the SMAD4-deficient or *SMAD4*-KD cells.

Altogether, these results reinforce the important role of *SMAD4* and TGFβ in the EMT process and PDA cancer metastasis; on the other hand, the absence of SMAD4 enhanced tumor stemness in our PDA model system.

We then further analyzed the possible role of the interplay between the TGFβ pathway and the biological clock in the formation of cancer metastasis. Interestingly, cell migration decreased upon *PER2* KD, but increased after *NR1D1* KD in SMAD4-proficient cells (Panc1, Figures 6A and 6C, ***p < 0.001, n = 3), in contrast to the results in SMAD4-deficient cells (AsPC1, Figures 6B and 6D, ***p < 0.001, n = 3). The TGFβ stimulation promoted the migration properties in clock genes KDs Panc1cells (Figure 6E,

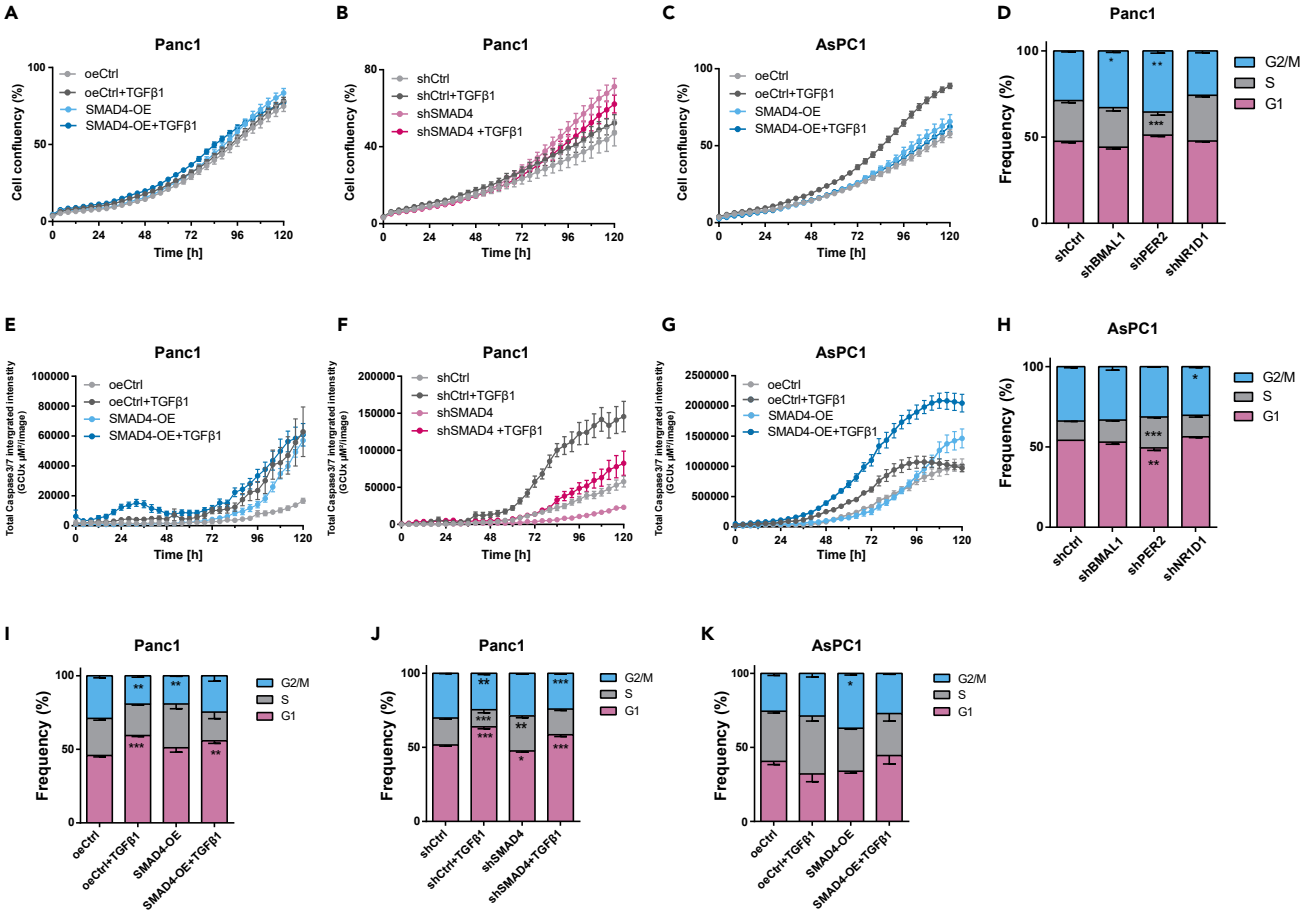

Figure 4. Clock Disruption and the Activation of the TGFβ/SMAD4 Pathway Affects Apoptosis and Cell Cycle in PDA Cells

(A–C) Proliferation analysis of PDA cells containing *SMAD4*-OE (A, C) or *SMAD4*-KD (B) constructs and their corresponding empty vectors (*shCtrl* or oeCtrl) stimulated with additional TGFβ1 (10ng/ml) or its solvent.(n = 8; mean ± SEM).

(E–G) Apoptosis analysis of PDA cell lines after *SMAD4*-OE (E, G) or *SMAD4*-KD (F) and their corresponding empty vectors (*shCtrl* or oeCtrl) with 24-h stimulation with TGFβ1 or its solvent (n = 3, mean ± SEM).

(D and H) Cell cycle measurements after clock gene KDs (sh*BMAL1*, sh*PER2*, sh*NR1D1)* and its empty control (*shCtrl*) in Panc1 (D) and AsPC1 (H) cells.

(I–K) Cell cycle measurements of *SMAD4*-KD and *SMAD4*-OE and corresponding control conditions (*shCtrl* and oeCtrl) in Panc1 (I, J) and AsPC1 (K) cells after a 24-h stimulation with TGFβ1 (10 ng/mL) or its solvent. (D and H–K) Phase distributions were compared with their respective control conditions (n =3, mean ± SEM, two-way ANOVA, *p < 0.05, **p < 0.01, ***p < 0.001).

See also Figures S5C, S5D, and S6.

*p < 0.05, **p < 0.01, ***p < 0.001, n = 3). TGFβ stimulation did not alter the migration ability of AsPC1 cells containing empty vectors (Figures 5F and 6F). On the other hand, TGFβ stimulation repressed migration in *shBMAL1* and *shPER2* and induced it in *shNR1D1* cells (Figure 6F, *p < 0.05, **p < 0.01, ***p < 0.001, n = 3), indicating that the interactions of the clock and the TGFβ non-canonical pathway may modify migration properties in SMAD4-deficient cells (AsPC1).

Therefore, we examined the expression level of clock genes after a 24-h TGFβ stimulation compared to Ctrl. We found that TGFβ stimulation upregulated *NR1D1* expression in AsPC1 (SMAD4-deficient) *NR1D1* KD cells (Figure S8D, ***p < 0.001, n = 3). Considering the decreased migration potential observed upon *NR1D1* KD (Figure 6B), the overexpression of *NR1D1* resulting from TGFβ stimulation (Figure S8D) might be the cause of the increase in migration in *NR1D1* KD cells (Figure 6F).

We further carried out trans-well invasion assays, which are more similar to the *in vivo* scenario. The results supported the conclusion from the migration assays (Figures 6G, 6H, 6K, and 6L).

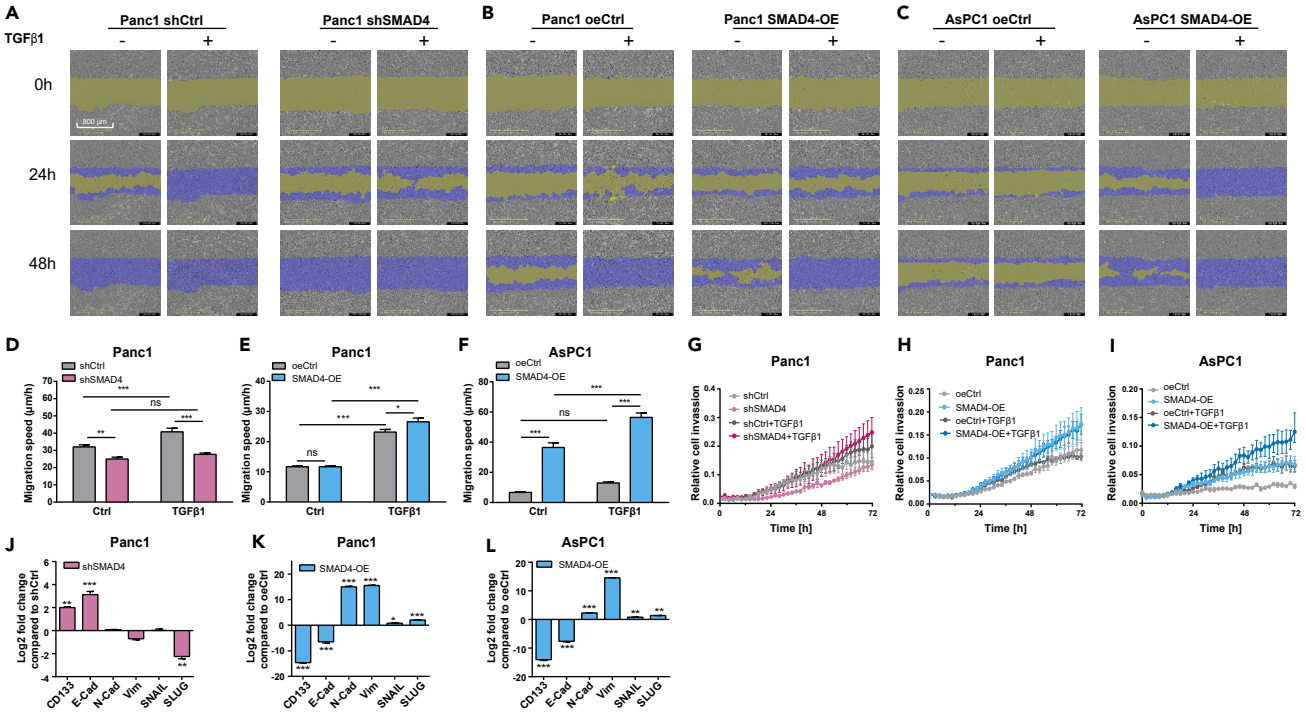

Figure 5. Migration and Invasion Analysis of *SMAD4*-KD and *SMAD4*-OE PDA Cells With or Without TGFβ1 Stimulations and Corresponding Expression Levels of EMT Markers

(A–C) Migration assays were performed with the IncuCyte S3 Live Cell System Analysis using a scratch wound assay. Partial representation of the scratch wound assay for *SMAD4*-KD (A) or *SMAD4*-OE (B, C) and their control (*shCtrl* and oeCtrl) conditions in PDA cells with additional TGFβ1 or its solvent stimulation at 0, 24, 48 h. Images were obtained with the IncuCyte S3 Software. Yellow mask indicates the wound boundaries. Blue mask indicates the initial scratch wound area.

(D–F) Average cell migration speed distribution in Panc1 (D, E) and AsPC1 (F) cells containing *SMAD4*-KD or *SMAD4*-OE constructs and their empty vectors (*shCtrl* and oeCtrl) with additional TGFβ1 or its solvent stimulation, ($n \geq 8$, mean ± SEM; two-way ANOVA, *$p < 0.05$, **$p < 0.01$, ***$p < 0.001$)..

(G–I) Invasion assays were carried out using a chemotaxis cell invasion assay for the IncuCyte S3 Live Cell System Analysis. Trans-well invasion assays for *SMAD4*-KD (G) or *SMAD4*-OE (H, I) and their control (*shCtrl* and oeCtrl) conditions in PDA cells were measured every 2h. Quantification was performed by measuring the total phase area of the bottom layer of the inner chamber within 72 h. Data were normalized for the initial value ($n \geq 6$, mean ± SEM).

(J–L) Expression levels of EMT and cancer stemness-related genes (*E-cadherin*, *N-cadherin*, *Vimentin*, *SNAIL*, *SLUG*,and *CD133*) in *SMAD4*-KD (J) or *SMAD4*-OE (K, L) conditions compared with their control conditions, *shCtrl* and oe-Ctrl respectively ($n = 3$, mean ± SEM, t test, *$p < 0.05$, **$p < 0.01$, ***$p < 0.001$). See also Figure S7.

We quantified the expression of *N-cadherin*, *E-cadherin*, *Vimentin, SNAIL,* and *SLUG*. Although the expression of *E-cadherin* was not significantly altered in *PER2* KD Panc1 cells, the expression of key MET (mesenchymal-epithelial transition, the reverse process of EMT) markers (*N-cadherin, Vimentin,* and *SLUG*) were significantly reduced, which hints toward initiation of MET in these cells, compared to the control cell line (Figures 6I and S8A, *$p < 0.05$, **$p < 0.01$, ***$p < 0.001$).

Although *N-cadherin* expression was not significantly altered (Figure 6I), the significant overexpression of *SNAIL* and *SLUG* in Panc1 cells upon *NR1D1* KD (Figure S8A) suggested that *NR1D1* KD initiated the EMT process in Panc1 cells, which is further supported by our results on migration and invasion. In AsPC1 cells, *N-cadherin* expression increased significantly upon *PER2* KD, whereas *NR1D1 KD* led to the downregulation of *SLUG* (Figures 6J and S8B, *$p < 0.05$, ***$p < 0.001$, $n = 3$). Thus, *PER2* KD triggered the EMT process in AsPC1 (SMAD4 deficient) cells, as supported by our results from the migration and invasion assays. Interestingly, *N-cadherin* was significantly increased, but *SLUG* was suppressed in AsPC1 *shBMAL1* cells (Figures 6J and S8, ***$p < 0.001$). However, there was no significant increase of the migration ability of *shBMAL1* when compared with *shCtrl* (Figure 6B). Furthermore, *CD133* was overexpressed in *PER2* KD for both PDA cell lines (Figures 6I and 6J, *$p < 0.05$), pointing to a role of *PER2* as a potential suppressor of tumor stemness in these cells.

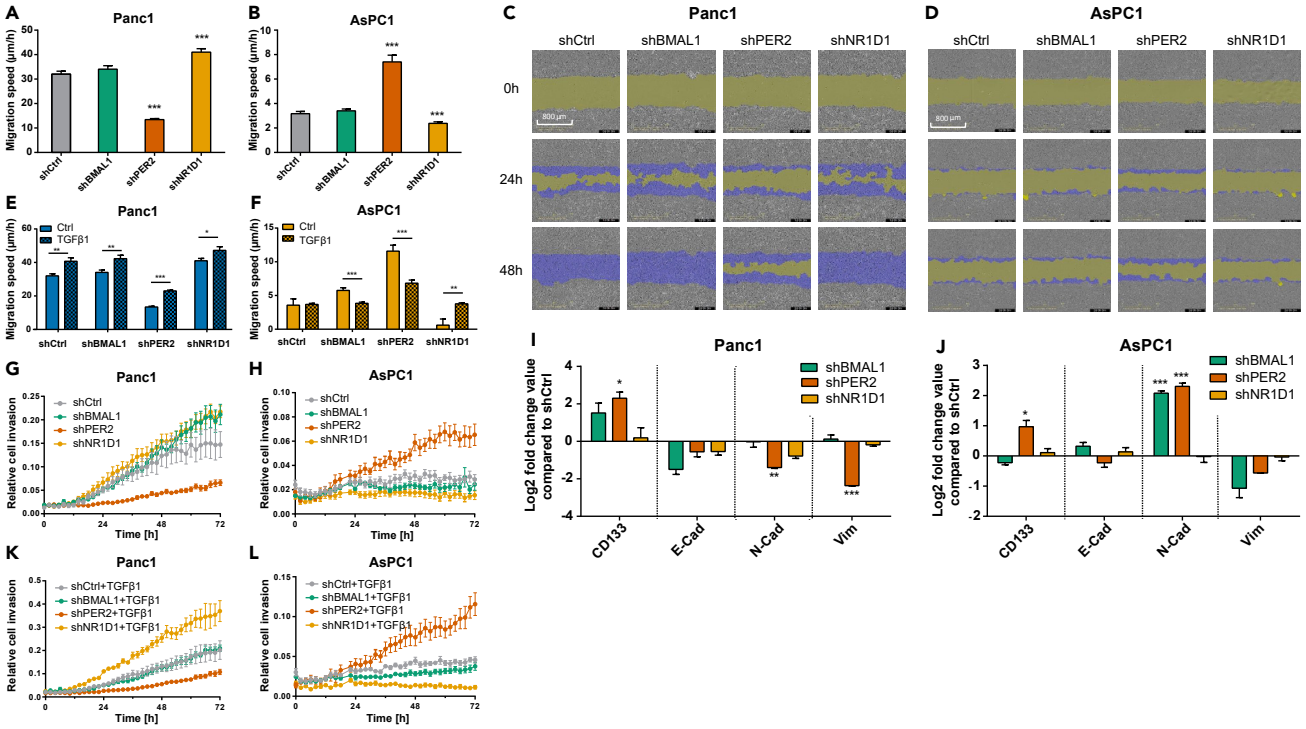

Figure 6. Dysregulation of Core-Clock Genes Affects Migration of Panc1 and AsPC1

(A, B, E, and F) Migration properties of *shCtrl* and knockdown cells (*shBMAL1*, *shPER2*, and *shNR1D1*) of Panc1 and AsPC1 with stimulation of TGFβ1 (10 ng/mL) or its solvent. Migration assays were performed using a scratch wound assay for the IncuCyte S3 Live Cell System Analysis. Average cell migration speed distribution from Panc1 and AsPC1 cells ($n \geq 8$, mean ± SEM; (A and B): one-way ANOVA; (E and F): t test, *$p < 0.05$, **$p < 0.01$, ***$p < 0.001$).

(C and D) Partial representation of the scratch wound assay for Panc1 (C) and AsPC1 (D) knockdown (*shBMAL1*, *shPER2* and *shNR1D1*) and control (*shCtrl*) cells at 0, 24, and 48 h. Images were obtained with the IncuCyte S3 Software. Yellow mask indicates the wound boundaries. Blue mask indicates the initial scratch wound area.

(G, H, K, and L) Invasion assays were carried out using a chemotaxis cell invasion assay for the IncuCyte S3 Live Cell System Analysis. Invasion assay for *shCtrl* and knockdown (*shBMAL1*, *shPER2* and *shNR1D1*) conditions in Panc1 (G, K) and AsPC1 (H, L) cells with or without TGFβ1 stimulation (10 ng/mL). Quantification was performed by measuring the total phase area of the bottom layer of the inner chamber within 72 h. Data were normalized to the initial value and presented as mean ± SEM, $n \geq 6$.

(I and J) mRNA levels of *CD133*, *Vimentin*, *E-cadherin*, and *N-cadherin* in PDA cells were analyzed after knockdown of core-clock genes (*shBMAL1*, *shPER2*, *shNR1D1*). Data shown as comparison to the *shCtrl* (mean ± SEM, n = 3, t test, *$p < 0.05$, **$p < 0.01$, ***$p < 0.001$).

See also Figure S8.

In addition, TGFβ impacts the expression of clock genes in a SMAD4-dependent manner (Figures S8C and S8D). *BMAL1* and *NR1D1* were upregulated in SMAD4-proficient cells (Panc1), and *PER2* was upregulated in SMAD4-deficient cells (AsPC1). These alterations on clock gene expression observed in *shCtrl* cells were not present upon *BMAL1* and *NR1D1* KDs in Panc1 and *PER2* KD in AsPC1. The expression of clock genes in AsPC1 *shBMAL1* revealed no significant difference with or without additional TGFβ. These results indicated that TGFβ upregulated the expression of core-clock genes differentially via the canonical and non-canonical pathway in our PDA cell model system.

The Knockdown of Core-Clock Genes and Modifications of the TGFβ Canonical Pathway Impact Treatment Response and Patient Survival

The main problem in current PDA standard therapy with gemcitabine is the rapid development of chemoresistance. Gemcitabine, an analog of deoxycytidine, leads to DNA fragmentation and cell death by inhibiting DNA chain elongation (Noble and Goa, 1997). We further investigated whether SMAD4 or clock dysfunction impacts the response of gemcitabine in our *vitro* model system. Our results showed that *SMAD4*-OE PDA cells were remarkably more sensitive to gemcitabine compared with oeCtrl, whereas *shSMAD4* cells were resistant to gemcitabine (Figures 7A–7C). Next, we explored the differential drug response of these two cell lines after core-clock gene KD. Although the gemcitabine IC50 of

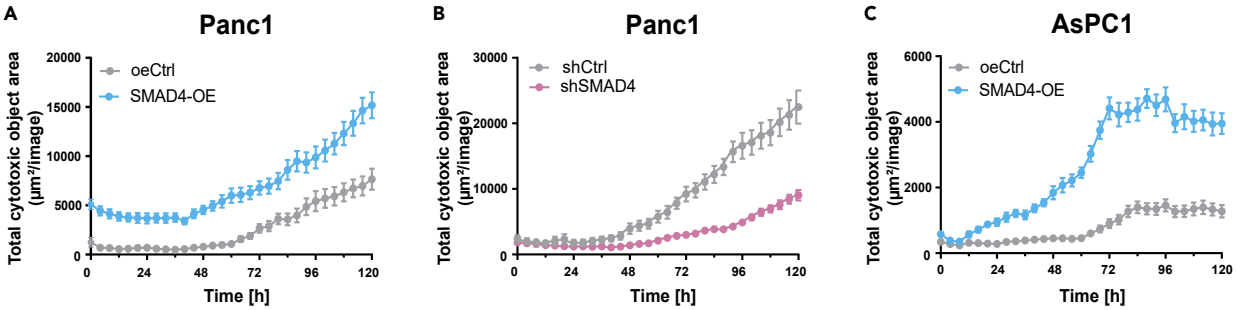
A
Panc1
Total cytotoxic object area (µm²/image)
oeCtrl
SMAD4-OE
Time [h]
B
Panc1
shCtrl
shSMAD4
Time [h]
C
AsPC1
oeCtrl
SMAD4-OE
Time [h]

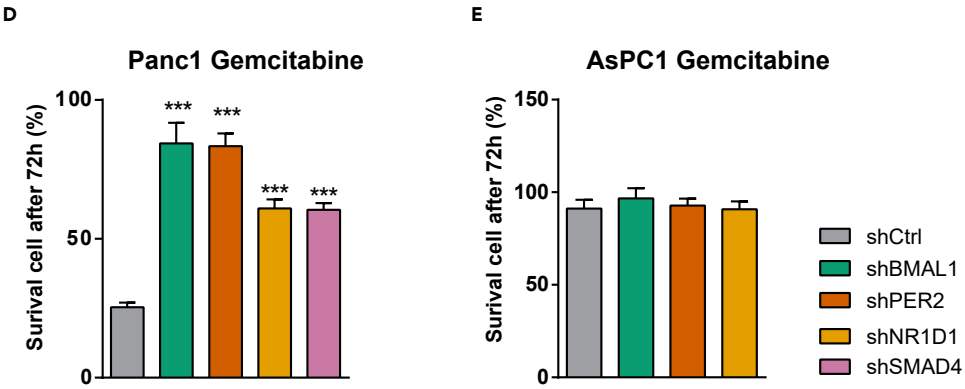
D
Panc1 Gemcitabine
Surival cell after 72h (%)
E
AsPC1 Gemcitabine
Surival cell after 72h (%)
shCtrl
shBMAL1
shPER2
shNR1D1
shSMAD4

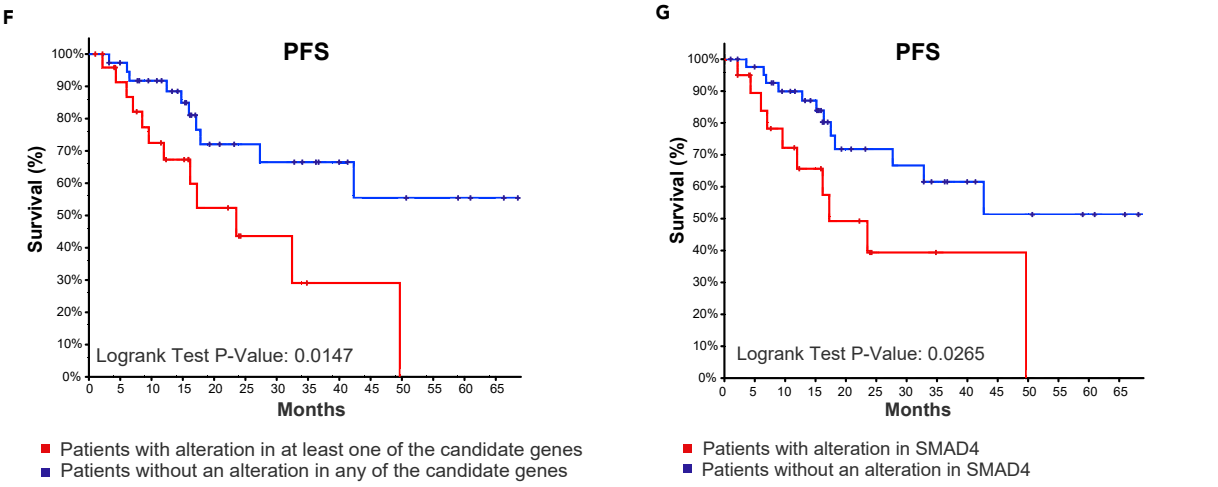
F
PFS
Survival (%)
Logrank Test P-Value: 0.0147
Months
Patients with alteration in at least one of the candidate genes
Patients without an alteration in any of the candidate genes
G
PFS
Survival (%)
Logrank Test P-Value: 0.0265
Months
Patients with alteration in SMAD4
Patients without an alteration in SMAD4

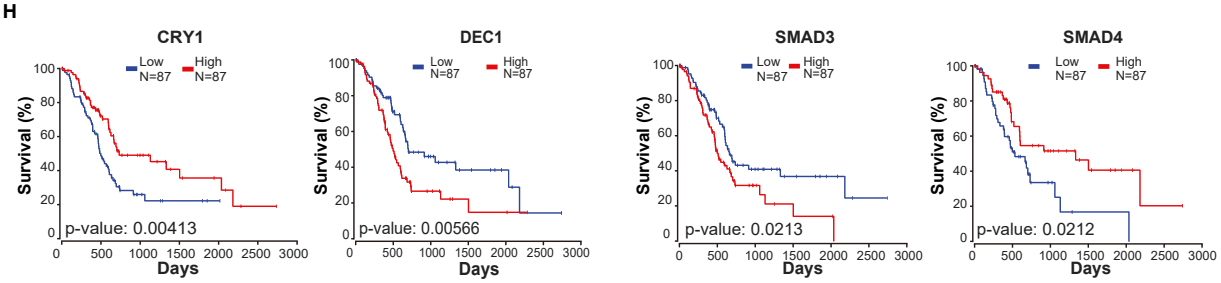
H
CRY1
Low N=87
High N=87
Survival (%)
p-value: 0.00413
Days
DEC1
p-value: 0.00566
SMAD3
p-value: 0.0213
SMAD4
p-value: 0.0212

Figure 7. The Downregulation of Core-Clock Genes and the Alteration of SMAD4 Expression Affects Drug Response in Panc1 and AsPC1 Cells

Cytotoxicity assays were performed using either an IncuCyte Red Cytotoxicity Reagent or NucLight Rapid Red Reagent for the IncuCyte S3 Live Cell System Analysis

(A–C) Cytotoxicity analysis for Panc1 (A, B) and AsPC1 (C) cells containing *SMAD4*-KD or *SMAD4*-OE constructs, in comparison with the corresponding empty controls (*shCtrl* and oeCtrl). 0 h after cell synchronization, gemcitabine was dissolved in IncuCyte Red Cytotoxicity Reagent and added to PDA cells (IC50: Panc1, 9.5 μM, and AsPC1, 23.9 μM). A cytotoxic index was calculated on IncuCyte S3 Live-Cell Analysis System in red phases. Data are expressed as mean ± SEM, n ≥ 6.

(D and E) Cytotoxicity analysis for Panc1 (D) and AsPC1 (E) cells containing knockdown constructs (*shBMAL1*, *shPER2* and *shNR1D1*) or its empty vector (*shCtrl*). Cell nuclei were labeled with NucLight Rapid Red Reagent. At 0 h after cell synchronization, gemcitabine (IC50: Panc1, 9.5 μM, and AsPC1, 23.9 μM) was added into the cells. 72 h after treatment, the number of viable cells per well was quantified with IncuCyte S3 Live-Cell Analysis System. Compared with the *shCtrl* (mean ± SEM, n = 6, one-way ANOVA, ***$p < 0.001$). See also Figure S9.

(F) Impact of alterations in our 10 candidate genes on progression-free survival (PFS) in a TCGA cohort of patients with pancreatic adenocarcinoma.

(G) Impact of SMAD4 mutation on PFS in a TCGA cohort of patients with pancreatic adenocarcinoma when compared with patients who do not have SMAD4 mutation (log rank $p < 0.05$).

(H) Impact of variation in candidate gene expression on overall survival in a TCGA cohort of patients with pancreatic adenocarcinoma. Survival curves were plotted using a Cox model that includes coxph (Surv (times, died) ~ gene + grade1 + grade2 + grade3 + age). Statistically significant results ($p < 0.05$) are shown in the figure. The project ID used for Kaplan Meier survival analysis (F and H) is retrieved from TCGA PAAD, dbGaP Study Accesion No: phs000178 (https://portal.gdc.cancer.gov/projects/TCGA-PAAD).

AsPC1(23.9μM) is much higher than that of Panc1 (9.5μM), AsPC1 *shCtrl* cells revealed higher viability after 72-h treatment when compared with Panc1 *shCtrl*. This further confirms an increased resistance to gemcitabine in the absence of SMAD4, in PDA cells. Unlike AsPC1, Panc1 clock gene KD cells showed significant resistance to gemcitabine treatment compared with *shCtrl* cells (Figures 7D and 7E, ***$p < 0.001$). These results emphasize the importance of circadian dysfunction in gemcitabine resistance in SMAD4-proficient PDA cells. The dysregulation of the circadian clock in Panc1 cells increased the resistant to gemcitabine, when compared with SMAD4-deficient cells (AsPC1), suggesting that SMAD4 impacts gene expression programs associated with the circadian clock and drug response in Panc1, which are distinct from AsPC1. These data highlight a novel role of the circadian clock in fine-tuning drug effectiveness in PDA with an emphasis on SMAD4. Moreover, to test whether drug administration at different times had different effects, we selected the time points 17, 20, and 23 h based on the time course RT-qPCR and bioluminescence data for the two cell lines, which show different expression of the core-clock genes measured (Figure S9A). Our data show that the timing of treatment administration has different effects in cell survival depending also on the additional perturbations generated to the cells. At particular times, the SMAD4-proficient PDA cells are more resistant to treatment, whereas for the SMAD4-deficient AsPC1 cells this effect was not observed (Figures S9B and S9C). After downregulation of SMAD4 in Panc1 (Figure S9B), the differential drug response to different treatment time points is significantly impaired. These results point to a role of SMAD4 in the time-dependent effect of treatment administration.

We then analyzed the impact of alterations in the clock genes *BMAL1*, *PER2*, *NR1D1*, *CRY1*, *DEC1*, and *DEC2*, as well as elements of the TGFβ pathway, *TGFβ1*, *SMAD3*, *SMAD4*, and *SMAD7* in patient survival. For that we quantified the mutational frequencies of these 10 genes from a cohort of patients with pancreatic adenocarcinoma (184 samples from the PanCancer study, Study Accession No: phs000178, https://portal.gdc.cancer.gov/projects/TCGA-PAAD) (Cancer Genome Atlas Research Network, 2017) curated from The Cancer Genome Atlas (TCGA) database. Among these candidate genes, *SMAD4* showed the highest mutation rate in the population (34%).

Patients with *SMAD4* mutation (mostly deletion) had a significant worse progression-free survival (PFS, $p < 0.05$) (Figure 7G). This suggested that *SMAD4* mutation in the advanced stage of the disease facilitates cancer progression. Interestingly if we compare the survival between the group of patients having no mutations for any of the candidate genes with the patients having mutations in at least one of the candidate genes, our results show a statistically significant influence on PFS ($p < 0.05$, Figure 7F). These results suggest that *SMAD4* mutation alone had a significant impact on the PFS, which is likely to be increased with the influence of additional mutations in our other candidate genes (Figures 7F and 7G).

To study the influence of alterations in gene expression for the set of genes described earlier in survival of patients, we performed a cox-regression-based survival analysis based on clinical parameters that include age, tumor grade, and gender in addition to the gene expression levels (Figure 7H). To evaluate high- and low-risk groups based on gene expression changes, we applied OncoLnc to 177 available mRNA datasets (RNA-Seq v.2) from the TCGA, Pancreatic Adenocarcinoma, patient cohort, which we divided into two

equal cohorts (N = 87 low, N = 87 high) representing high- and low-expression groups, respectively (Figure 7H). The clock genes *CRY1* and *DEC1*, and TGFβ signaling family members *SMAD3* and *SMAD4*, showed significant impact on survival (Figure 7H, log rank test $p < 0.05$) for PDA patients suggesting a potential clinical value for targeting these genes in a therapeutic context. Together with the results from our *in vitro* model, the expression of the clock genes *DEC1* and *CRY1* also revealed a SMAD4 dependency. These data highlight an important role for the cross-talk between the endogenous molecular clock and the TGFβ canonical pathway and its likely contribution to the progression and prognosis of PDA.

DISCUSSION

A dysregulated clock in patients with cancer was shown to be associated with poorer prognosis and a shorter lifespan. Pancreatic cancer is one of the major causes of cancer mortality worldwide. Several studies have identified disruptions in clock genes, which are correlated with cancer progression in pancreatic cancer (Jiang et al., 2016; Relles et al., 2013; Tavano et al., 2015; Wu et al., 2012). Among these genes are members of the core-clock machinery (*BMAL1* and *PER2*), as well as clock-regulated genes (*SIRT1* and *DEC1*), which either show abnormal expression or altered rhythmic pattern resulting in cancer progression and EMT (Jiang et al., 2016; Relles et al., 2013; Tavano et al., 2015; Wu et al., 2012). However, the detailed mechanism of circadian clock regulation in pancreatic cancer is still unclear. TGFβ is involved in oncogenic transformation and cancer progression, and it plays a vital role in cancer homeostasis. As tumors grow and progress, genetic alterations often occur on TGFβ canonical signaling components (including SMAD4 mutations), leading to the activation of pro-oncogenic pathways such as RAS, PI3K, and MAPK (Principe et al., 2017). These genetic modifications eventually override the growth inhibitory effects of the TGFβ canonical pathway, further contributing to tumor development. Although it is known that elements of TGFβ canonical pathway are involved in circadian regulation (Akagi et al., 2017; Chen et al., 2015; Sato et al., 2019), the molecular mechanisms underlying this cross-talk in human cancers remain largely uncharacterized.

In the present study, we first characterized the circadian phenotype of pancreatic cancer cells, with similar proliferation profiles, originated from a primary tumor (Panc1) and metastasis ascites (AsPC1). The cells derived from the primary tumor show a differential clock phenotype when compared with the cells derived from the metastasis ascites, pointing to a differential regulation of the clock machinery in different types, genomic background, and stages of cancer, in agreement with previous reports for other cancer types (Fuhr et al., 2018; Relogio et al., 2014).

To explore the possible mechanisms connecting the circadian clock and tumor progression in pancreatic cancer, we focused on the CCG SMAD4. As the core mediator of the TGFβ canonical pathway, SMAD4 is known to assist the modulation of cancer progression (reviewed in Xu et al., (2009)). We hypothesized that SMAD4 could affect the circadian phenotype and subsequently malignant phenotypes of PDA cells. Hence, we established a pancreatic cancer *in vitro* model consisting of SMAD4-positive (Panc1) and SMAD4-negative (AsPC1) cell lines and investigated this interplay through gene knockdown and overexpression of core-clock elements, TGFβ and SMAD4. Our data show that *TGFβ1*, *SMAD3*, *SMAD4*, and *SMAD7* exhibit circadian oscillation at the transcript level in Panc1 cells, pointing to the circadian regulation of the TGFβ pathway in SMAD4-proficient PDA cells. Chen et al. reported that the transcript of *TGFβ1* oscillates in a circadian fashion in mouse embryonic fibroblasts, whereas the oscillation is perturbed in *Clock*-deficient mice (Chen et al., 2015). Furthermore, the authors showed that binding of the Bmal1-Clock heterodimer to *mTGFβ1* exhibits a circadian rhythmicity in mouse renal cells (Chen et al., 2015). Another study showed enriched Bmal1 binding on promoter regions of *TGFβ1* and *Smad3*, which occurred at the similar time as Bmal1 E-box binding to Nr1d1 (at CT8) in mouse brown adipocytes (Nam et al., 2015). These results indicate that Bmal1 activates the expression of components of the TGFβ canonical pathway (via TGFβ1 and Smad3) in parallel with the activation of Nr1d1. However, whether mRNA dynamics of TGFβ signaling elements are under the circadian modulation in human cancers is still largely uncharacterized. Interestingly, our results show that the circadian oscillation (period of circa 24 h) of elements of the TGFβ pathway is only detectable in SMAD4-positive cells and not in SMAD4-deficient cells. In the absence of extrinsic TGFβ, transcription of *SMAD7* can be induced by the intrinsic TGFβ following a circadian pattern. *TGFβ1* transcript also shows a similar period with a different phase than *SMAD7*. This further suggests that autocrine TGFβ may activate the transcription of *SMAD7* in a circadian fashion. We also detected circadian rhythms in *BMAL1* mRNA of SMAD4-positive cells, resembling our observation in transcripts of

TGFβ canonical elements (*SMAD3* and *TGFB1*). This supported our hypothesis that SMAD4 may serve as a mediator element bridging the clock and the TGFβ signaling pathway.

It has been previously shown that the core-clock genes *Bmal1* and *Nr1d1* are involved in the TGFβ canonical pathway in mouse brown adipose (Nam et al., 2015). In agreement, we show that clock perturbation via small hairpin RNA knockdown of core-clock elements (*BMAL1* and *NR1D1*) resulted in abolished oscillations of *TGFβ1*, *SMAD3, SMAD4,* and *SMAD7*, confirming the existence of bidirectional connection between core-clock elements and the TGFβ canonical pathway in human PDA cells. In addition, the transcription factors, DEC1 and DEC2, inhibit *PER* via protein-protein interactions with BMAL1 and/or competition for E-box elements (Honma et al., 2002). Of note, DEC1/2 is a downstream element of TGFβ canonical pathway as well (Adorno et al., 2009; Kon et al., 2008; Prunier et al., 2019; Zawel et al., 2002). To identify the specific bridging elements between the core-clock and the TGFβ signaling, we further analyzed the expression of the clock genes *DEC1* and *DEC2* (Figures 2D, 2G, and 2J). We observed a negative correlation between *SMAD4* and *DEC1/2* expression through *SMAD4* downregulation and overexpression assays, which reinforced the mediating role of DEC1/2 via TGFβ pathway in regulating the circadian clock.

We further investigated whether TGFβ activation and *SMAD4* expression could affect the oscillatory phenotype of *BMAL1* and *PER2* promoter activity in both SMAD4-positive and SMAD4-deficient pancreatic cancer cell lines using live bioluminescence recordings. Surprisingly, TGFβ stimulation alone did not cause major changes in the period of oscillations for both cell lines. However, the period was significantly shorter when we combined TGFβ stimulation with *SMAD4* overexpression in both cell lines, indicating that the TGFβ-clock interplay might be *SMAD4* dependent.

Downregulation of core-clock genes resulted in an overall higher proliferative and apoptotic activity in SMAD4-positive cells. Of note, *SMAD4* downregulation only affected cell proliferation and not apoptosis in these cells. We speculate that reduced expression of *SMAD4* might activate the non-SMAD TGFβ signaling pathway, including the MAPK/ERK, resulting in higher cell proliferation and growth (reviewed in Zhang, 2017). We confirmed the activation of the Ras-mediated TGFβ non-canonical pathway by measuring the expression of RAS and p-ERK, and particularly after stimulation with TGFβ, further pointing to the activation of the RAS/ERK pathway.

In SMAD4-deficient cells, the apoptotic rate was also increased upon knockdown of clock genes. However, cell proliferation was only notably increased upon *PER2* downregulation in AsPC1. Our cell cycle analysis also confirmed this finding showing higher percentage of *shPER2* cells in the S phase. The overall differential proliferative properties and cell cycle distributions upon the KD of clock genes in both PDA cells suggest that cell fate determination via the clock is altered in SMAD4 mutant (AsPC1) cells. *SMAD4* overexpression, on the other hand, resulted in remarkably higher cellular apoptosis in both cell lines. This confirms the apoptotic role of the canonical TGFβ signaling pathway mediated by SMAD4, as described in previous studies, and hints to the central role of *SMAD4* in regulating the canonical TGFβ signaling pathway (Du et al., 2018; Pang et al., 2011). This effect is more evident in our SMAD4-deficient cells, with a notable increase in apoptosis upon *SMAD4* overexpression with additional TGFβ1 stimulation.

Previous reports indicate a prominent role for the TGFβ signaling pathway in regulating cell cycle progression (Buenemann et al., 2001; Mukherjee et al., 2010; Voss et al., 1999). Indeed, we showed in our PDA model that cell-cycle arrest was triggered when cells were stimulated with TGFβ and *SMAD4* was overexpressed. We observed an opposite effect after *SMAD4* downregulation resulting in more S-phase cells and proliferation. Furthermore, TGFβ stimulation alone inhibited G1/S cell cycle propagation only in SMAD4-positive cells. These results highlight the determinant role of SMAD4 in regulating cell cycle proliferation and apoptosis via downstream genes of TGFβ canonical and non-canonical signaling pathway (e.g., *P21*, *c-MYC,* and *RAS*) (Alexandrow and Moses, 1995; Mukherjee et al., 2010; Principe et al., 2017; Voss et al., 1999), further pointing to a differential regulation of TGFβ pathway in different stages of pancreatic cancer, as reported in the present or former studies in a SMAD4-dependent manner.

Regulating EMT and cell invasion is one of the key functions of TGFβ signaling pathway in cancer cells (Lee et al., 2013; Xu et al., 2009). Cells undergoing EMT lose expression of E-cadherin and other components needed for epithelial cell junction stability and are able to produce a mesenchymal cell cytoskeleton acquiring motility and invasive properties (Massague, 2008). The reverse process of EMT, MET, involves

the activation of E-cadherin and suppression of N-cadherin (Yao et al., 2011). Hence, we analyzed migration/invasion properties upon *SMAD4* expression and TGFβ stimulation in both cell models. TGFβ stimulation alone was sufficient to enhance cell migration in SMAD4-positive cells, whereas in SMAD4-deficient cells, both *SMAD4* overexpression and TGFβ stimulation resulted in the highest migratory and invasion activities, suggesting that *SMAD4* expression is necessary for enhancing cancer metastasis. We confirmed this finding through *SMAD4* downregulation and showed that cell migration was not affected upon TGFβ stimulation. After measuring the expression of EMT marker genes (e.g., *E-Cad, N-Cad, SNAIL, SLUG*) in pancreatic cancer (Takano et al., 2007), we found that *SMAD4* overexpression reduced the expression of epithelial marker genes (*E-Cad*) and enhanced the expression of genes involved in mesenchymal transition (*N-Cad, Vim, SNAIL,* and *SLUG*) in both cell lines, indicating that *SMAD4* mediates invasion by regulating the expression of key marker genes involved in EMT. We observed the opposite effect in EMT gene expression after *SMAD4* knockdown, which reinforces the role of SMAD4 in cancer invasion. In addition, we sought to explore another cancer hallmark, tumor stemness via the analysis of *CD133* (Tabu et al., 2010). In our model system, we observed a downregulation of *CD133* in PDA cells with *SMAD4* overexpression. More interestingly, increased *CD133* expression after *SMAD4* KD implied the acquisition of cancer stem-like hallmark in our study, in agreement with previous studies (Chen et al., 2014).

Cancer metastasis is the cumulative result of multiple changes in tumor cells and their microenvironment. Cell migration was differentially regulated in SMAD4-positive and SMAD4-deficient cells upon *PER2* and *NR1D1* downregulation (Figure 6). In SMAD4-positive cells, cell migration was decreased upon *PER2* knockdown and increased after *NR1D1* downregulation, whereas we observed an opposite effect in the cell line deficient for SMAD4. Interestingly, TGFβ activation also implied an overall opposite effect in the core-clock knockdown cells from SMAD4-positive and SMAD4-negative PDA: promoting migration in Panc1 cells and inhibiting it in AsPC1 cells. These results show that cancer cell properties seem to be *SMAD4*-dependent upon clock dysregulation, highlighting the reciprocal role of the circadian clock and *SMAD4* in pancreatic cancer. Notably, the downregulation of *PER2* results in the increased expression of *CD133* in both PDA cells, hinting at the crucial role of PER2 in cancer stemness independent of SMAD4 (Katamune et al., 2019). Hence, based on our results on proliferation, apoptosis, cell cycle, and cellular metastatic proprieties, we speculated that TGFβ might alter the circadian clock differently via the canonical (in Panc1) and non-canonical (in AsPC1) pathways.

Finally, we tested whether treatment response in pancreatic cancer is clock and/or SMAD4 dependent. Results from previous clinical trials concluded that the loss of SMAD4 is a negative prognostic indicator, which is strongly associated with poor chemosensitivity (Shin et al., 2017; Singh et al., 2012; Yamada et al., 2015). Extrinsic DNA damage due to gemcitabine administration imposes threats to cellular homeostasis involving the regulation of both the TGFβ signaling pathway (Li et al., 2019; Liu et al., 2019) and clock components (Jiang et al., 2018; Ka et al., 2017; Mazzoccoli et al., 2016; Sulli et al., 2018). To elucidate the molecular mechanisms that drive chemoresistance in this PDA model, we hypothesized that during the exposure to gemcitabine, clock genes and TGFβ canonical components participate in the regulation of DNA repair, as well as in the maintenance of genomic stability.

A previous study showed that patients with PDA with SMAD4 loss have poorer PFS in the gemcitabine-based treatment subgroup (Ormanns et al., 2017). Consistently, we observed that SMAD4-deficient cells are resistant to the chemotherapy with gemcitabine. Although the intrinsic mechanism has not been fully understood yet, based on our apoptosis and cell cycle data, we assume that it relates to the effect in the cell cycle due to the anti-apoptotic role of SMAD4.

Clock perturbation via the knockdown of core-clock genes aggravates chemoresistance, notably only in SMAD4-proficient pancreatic cancer cells. Associated with the fact that genetic alterations (mostly inactivation) of SMAD4 often occur in the advanced stage of pancreatic cancers, we concluded that the molecular clock functions as a repressor of chemoresistance of gemcitabine while SMAD4 is not mutated (e.g., cancers in the early stage). Hence, loss of Smad4 function along with TGFβ stimulation (as observed for AsPC1, SMAD4-deficient cells) activates the non-canonical pathway (RAS) and increases CSCs (CD133 upregulation), further contributing to the acquisition of malignant properties and drug resistance. These findings highlight the important role of SMAD4 in affecting gene expression programs associated with the circadian clock and drug response in SMAD4-proficient cells, which are distinct from those in SMAD4-deficient cells. Furthermore, our results emphasize the importance of circadian clock dysfunction in gemcitabine resistance in SMAD4-proficient PDA cells. Our

data indicate that drug response and cell fate determination in pancreatic cancer cells with WT or mutated SMAD4, upon the dysregulation of the circadian clock, resulted in a significant differential change in cell survival rate and invasiveness, highlighting the importance of the associations between the TGFβ canonical pathway, biological clock, and drug timing affecting chemosensitivity in a cancer context.

The information that we obtained from our *in vitro* model system aids to the understanding of the impact of the clock in the SMAD4 network and consequently in cell fate decisions. In addition, and to better show the potential of our results beyond the *in vitro* experiments presented, we performed a computational analysis with publicly available datasets for patients with pancreatic cancer. In our PDA model system, the overexpression of *SMAD4* resulted in upregulation of *CRY1* and downregulation of *DEC1*; the downregulation of *SMAD4* led to suppression of *CRY1* and overexpression of *DEC1*. These results agree with our survival analysis for a cohort of patients with PDA that indicated a better prognosis (PFS, $p < 0.05$) for the groups of patients with high expression of *CRY1*, low expression of *DEC1*, and high expression of *SMAD4*. In addition, the genomic alteration of *SMAD4* (mostly deletion) alone led to a worse PFS ($p = 0.0265$), which is aggravated when combined with alterations of other genes bridging the clock and the TGFβ canonical pathway ($p = 0.0147$). This points to a relevant role of the molecular clock, together with the TGFβ pathway, in contributing to the progression and prognosis of PDA. Altogether, our data show that the circadian clock regulates the TGFβ/SMAD4 pathway in PDA cells with likely consequences on cancer progression (invasion and EMT) and patient survival and suggest a profound role for SMAD4 as an intermediate component linking the clock machinery to the TGFβ pathway. This information may be relevant for patients with pancreatic cancer undergoing chemotherapy to increase the effectiveness of the therapy based on SMAD4 mutation and the circadian clock.

Limitations of the Study

We consider the lack of *in vivo* data as a limitation of our study, with the caveat that mice (as nocturnal animals) have a different clock compared with humans (as diurnal animals) and hence results from an *in vivo* mouse model regarding alteration of the circadian clock may not be directly relevant or properly translated to human disease models. This is particularly relevant when comparing drug timing, drug toxicity, and drug efficacy between nocturnal and diurnal models (reviewed in Dallmann et al., 2016). In addition, we have previously shown that in circadian studies, the host-cancer interaction in *in vivo* models (using xenografts) has an impact on the circadian phenotype of the xenograft, which adds complexity to the interpretation of the results with regards to the circadian machinery (Basti et al., 2020).

Resource Availability

Lead Contact

Further information and requests for resources and reagents should be directed to and will be fulfilled by the Lead Contact, Dr. Angela Relógio (angela.relogio@charite.de).

Materials Availability

This study did not generate new unique reagents.

Data and Code Availability

This study did not generate datasets/code.

METHODS

All methods can be found in the accompanying Transparent Methods supplemental file.

SUPPLEMENTAL INFORMATION

Supplemental Information can be found online at https://doi.org/10.1016/j.isci.2020.101551.

ACKNOWLEDGMENTS

We thank Dr. Rosa Schmuck from the Chirurgischen Klinik, Charité – Universitätsmedizin Berlin, for providing the cell lines, and Dr. Sam Thiagalingam from the department of medicine, Boston University, for providing pBabe-puro-Smad4-Flag. The work in A.R.'s group was funded by the German Federal Ministry of Education and Research (BMBF)—eBio-CIRSPLICE - FKZ031A316, and by the Dr. Rolf M. Schwiete

Stiftung. Y.L. was additionally funded by Jinan Huaiyin Hospital of Shandong Province. Y.L., A.B., and M.Y. were additionally funded by the Berlin School of Integrative Oncology (BSIO) of the Charité – Universitätsmedizin Berlin. We acknowledge support from the German Research Foundation (DFG) and the Open Access Publication Fund of Charité – Universitätsmedizin Berlin.

AUTHOR CONTRIBUTIONS

Conceptualization, A.R.; Methodology, A.R. and Y.L.; Investigation, Y.L., A.B., and M.Y.; Validation, Y.L., A.B., and A.R.; Writing – Original Draft, Y.L., A.B., and A.R.; Writing – Review & Editing, Y.L., A.B., M.Y., and A.R.; Funding Acquisition, A.R.; Resources, A.R.; Supervision, A.R.

DECLARATION OF INTERESTS

The authors declare that they have no conflict of interest.

Received: March 16, 2020
Revised: June 24, 2020
Accepted: September 9, 2020
Published: October 23, 2020

REFERENCES

Abreu, M., Basti, A., Genov, N., Mazzoccoli, G., and Relogio, A. (2018). The reciprocal interplay between TNFalpha and the circadian clock impacts on cell proliferation and migration in Hodgkin lymphoma cells. Sci. Rep. *8*, 11474.

Adorno, M., Cordenonsi, M., Montagner, M., Dupont, S., Wong, C., Hann, B., Solari, A., Bobisse, S., Rondina, M.B., Guzzardo, V., et al. (2009). A Mutant-p53/Smad complex opposes p63 to empower TGFbeta-induced metastasis. Cell *137*, 87–98.

Akagi, R., Akatsu, Y., Fisch, K.M., Alvarez-Garcia, O., Teramura, T., Muramatsu, Y., Saito, M., Sasho, T., Su, A.I., and Lotz, M.K. (2017). Dysregulated circadian rhythm pathway in human osteoarthritis: NR1D1 and BMAL1 suppression alters TGF-beta signaling in chondrocytes. Osteoarthr. Cartil. *25*, 943–951.

Alexandrow, M.G., and Moses, H.L. (1995). Transforming growth factor beta and cell cycle regulation. Cancer Res. *55*, 1452–1457.

Basti, A., Fior, R., Yalin, M., Povoa, V., Astaburuaga, R., Li, Y., Naderi, J., Godinho Ferreira, M., and Relogio, A. (2020). The core-clock gene NR1D1 impacts cell motility in vitro and invasiveness in A zebrafish xenograft colon cancer model. Cancers (Basel) *12*, 853.

Berrozpe, G., Schaeffer, J., Peinado, M.A., Real, F.X., and Perucho, M. (1994). Comparative analysis of mutations in the p53 and K-ras genes in pancreatic cancer. Int. J. Cancer *58*, 185–191.

Buenemann, C.L., Willy, C., Buchmann, A., Schmiechen, A., and Schwarz, M. (2001). Transforming growth factor-beta1-induced Smad signaling, cell-cycle arrest and apoptosis in hepatoma cells. Carcinogenesis *22*, 447–452.

Cancer Genome Atlas Research Network (2017). Integrated genomic characterization of pancreatic ductal adenocarcinoma. Cancer Cell *32*, 185–203 e113.

Chen, W.D., Yeh, J.K., Peng, M.T., Shie, S.S., Lin, S.L., Yang, C.H., Chen, T.H., Hung, K.C., Wang, C.C., Hsieh, I.C., et al. (2015). Circadian CLOCK mediates activation of transforming growth factor-beta signaling and renal fibrosis through cyclooxygenase 2. Am. J. Pathol. *185*, 3152–3163.

Chen, Y.W., Hsiao, P.J., Weng, C.C., Kuo, K.K., Kuo, T.L., Wu, D.C., Hung, W.C., and Cheng, K.H. (2014). SMAD4 loss triggers the phenotypic changes of pancreatic ductal adenocarcinoma cells. BMC Cancer *14*, 181.

Cheng, T., Shen, H., Rodrigues, N., Stier, S., and Scadden, D.T. (2001). Transforming growth factor beta 1 mediates cell-cycle arrest of primitive hematopoietic cells independent of p21(Cip1/Waf1) or p27(Kip1). Blood *98*, 3643–3649.

Coveler, A.L., Rossi, G.R., Vahanian, N.N., Link, C., and Chiorean, E.G. (2016). Algenpantucel-L immunotherapy in pancreatic adenocarcinoma. Immunotherapy *8*, 117–125.

Dallmann, R., Okyar, A., and Levi, F. (2016). Dosing-time makes the poison: circadian regulation and pharmacotherapy. Trends Mol. Med. *22*, 430–445.

Davis, K., Roden, L.C., Leaner, V.D., and van der Watt, P.J. (2019). The tumour suppressing role of the circadian clock. IUBMB Life *71*, 771–780.

Di Micco, R., Sulli, G., Dobreva, M., Liontos, M., Botrugno, O.A., Gargiulo, G., dal Zuffo, R., Matti, V., d'Ario, G., Montani, E., et al. (2011). Interplay between oncogene-induced DNA damage response and heterochromatin in senescence and cancer. Nat. Cell Biol *13*, 292–302.

Du, X., Pan, Z., Li, Q., Liu, H., and Li, Q. (2018). SMAD4 feedback regulates the canonical TGF-beta signaling pathway to control granulosa cell apoptosis. Cell Death Dis. *9*, 151.

El-Athman, R., Genov, N.N., Mazuch, J., Zhang, K., Yu, Y., Fuhr, L., Abreu, M., Li, Y., Wallach, T., Kramer, A., et al. (2017). The Ink4a/Arf locus operates as a regulator of the circadian clock modulating RAS activity. PLoS Biol. *15*, e2002940.

Fuhr, L., Abreu, M., Pett, P., and Relogio, A. (2015). Circadian systems biology: when time matters. Comput. Struct. Biotechnol. J. *13*, 417–426.

Fuhr, L., El-Athman, R., Scrima, R., Cela, O., Carbone, A., Knoop, H., Li, Y., Hoffmann, K., Laukkanen, M.O., Corcione, F., et al. (2018). The circadian clock regulates metabolic phenotype rewiring via HKDC1 and modulates tumor progression and drug response in colorectal cancer. EBioMedicine *33*, 105–121.

Gery, S., Gombart, A.F., Yi, W.S., Koeffler, C., Hofmann, W.K., and Koeffler, H.P. (2005). Transcription profiling of C/EBP targets identifies Per2 as a gene implicated in myeloid leukemia. Blood *106*, 2827–2836.

Glumac, P.M., and LeBeau, A.M. (2018). The role of CD133 in cancer: a concise review. Clin. Transl. Med. *7*, 18.

Honma, S., Kawamoto, T., Takagi, Y., Fujimoto, K., Sato, F., Noshiro, M., Kato, Y., and Honma, K. (2002). Dec1 and Dec2 are regulators of the mammalian molecular clock. Nature *419*, 841–844.

Jiang, W., Zhao, S., Jiang, X., Zhang, E., Hu, G., Hu, B., Zheng, P., Xiao, J., Lu, Z., Lu, Y., et al. (2016). The circadian clock gene Bmal1 acts as a potential anti-oncogene in pancreatic cancer by activating the p53 tumor suppressor pathway. Cancer Lett. *371*, 314–325.

Jiang, W., Zhao, S., Shen, J., Guo, L., Sun, Y., Zhu, Y., Ma, Z., Zhang, X., Hu, Y., Xiao, W., et al. (2018). The MiR-135b-BMAL1-YY1 loop disturbs pancreatic clockwork to promote tumourigenesis and chemoresistance. Cell Death Dis. *9*, 149.

Ka, N.L., Na, T.Y., Na, H., Lee, M.H., Park, H.S., Hwang, S., Kim, I.Y., Seong, J.K., and Lee, M.O. (2017). NR1D1 recruitment to sites of DNA damage inhibits repair and is associated with chemosensitivity of breast cancer. Cancer Res. *77*, 2453–2463.

Katamune, C., Koyanagi, S., Hashikawa, K.I., Kusunose, N., Akamine, T., Matsunaga, N., and Ohdo, S. (2019). Mutation of the gene encoding the circadian clock component PERIOD2 in oncogenic cells confers chemoresistance by up-regulating the Aldh3a1 gene. J. Biol. Chem. *294*, 547–558.

Kita, K., Saito, S., Morioka, C.Y., and Watanabe, A. (1999). Growth inhibition of human pancreatic cancer cell lines by anti-sense oligonucleotides specific to mutated K-ras genes. Int. J. Cancer *80*, 553–558.

Kon, N., Hirota, T., Kawamoto, T., Kato, Y., Tsubota, T., and Fukada, Y. (2008). Activation of TGF-beta/activin signalling resets the circadian clock through rapid induction of Dec1 transcripts. Nat. Cell Biol *10*, 1463–1469.

Lamouille, S., Xu, J., and Derynck, R. (2014). Molecular mechanisms of epithelial-mesenchymal transition. Nat. Rev. Mol. Cell Biol. *15*, 178–196.

Lee, J., Choi, J.H., and Joo, C.K. (2013). TGF-beta1 regulates cell fate during epithelial-mesenchymal transition by upregulating survivin. Cell Death Dis. *4*, e714.

Lehmann, R., Childs, L., Thomas, P., Abreu, M., Fuhr, L., Herzel, H., Leser, U., and Relogio, A. (2015). Assembly of a comprehensive regulatory network for the mammalian circadian clock: a bioinformatics approach. PLoS One *10*, e0126283.

Li, Y., Liu, Y., Chiang, Y.J., Huang, F., Li, Y., Li, X., Ning, Y., Zhang, W., Deng, H., and Chen, Y.G. (2019). DNA damage activates TGF-beta signaling via ATM-c-cbl-mediated stabilization of the type II receptor TbetaRII. Cell Rep. *28*, 735–745.e734.

Lieber, M., Mazzetta, J., Nelson-Rees, W., Kaplan, M., and Todaro, G. (1975). Establishment of a continuous tumor-cell line (panc-1) from a human carcinoma of the exocrine pancreas. Int. J. Cancer *15*, 741–747.

Liu, Q., Lopez, K., Murnane, J., Humphrey, T., and Barcellos-Hoff, M.H. (2019). Misrepair in context: TGFbeta regulation of DNA repair. Front. Oncol. *9*, 799.

Mao, L., Dauchy, R.T., Blask, D.E., Slakey, L.M., Xiang, S., Yuan, L., Dauchy, E.M., Shan, B., Brainard, G.C., Hanifin, J.P., et al. (2012). Circadian gating of epithelial-to-mesenchymal transition in breast cancer cells via melatonin-regulation of GSK3beta. Mol. Endocrinol. *26*, 1808–1820.

Massague, J. (2008). TGFbeta in cancer. Cell *134*, 215–230.

Mazzoccoli, G., Colangelo, T., Panza, A., Rubino, R., De Cata, A., Tiberio, C., Valvano, M.R., Pazienza, V., Merla, G., Augello, B., et al. (2016). Deregulated expression of cryptochrome genes in human colorectal cancer. Mol. Cancer *15*, 6.

Mukherjee, P., Winter, S.L., and Alexandrow, M.G. (2010). Cell cycle arrest by transforming growth factor beta1 near G1/S is mediated by acute abrogation of prereplication complex activation involving an Rb-MCM interaction. Mol. Cell Biol. *30*, 845–856.

Nam, D., Guo, B., Chatterjee, S., Chen, M.H., Nelson, D., Yechoor, V.K., and Ma, K. (2015). The adipocyte clock controls brown adipogenesis through the TGF-beta and BMP signaling pathways. J. Cell Sci. *128*, 1835–1847.

Noble, S., and Goa, K.L. (1997). Gemcitabine. A review of its pharmacology and clinical potential in non-small cell lung cancer and pancreatic cancer. Drugs *54*, 447–472.

Ormanns, S., Haas, M., Remold, A., Kruger, S., Holdenrieder, S., Kirchner, T., Heinemann, V., and Boeck, S. (2017). The impact of SMAD4 loss on outcome in patients with advanced pancreatic cancer treated with systemic chemotherapy. Int. J. Mol. Sci. *18*, 1094.

Pang, L., Qiu, T., Cao, X., and Wan, M. (2011). Apoptotic role of TGF-beta mediated by Smad4 mitochondria translocation and cytochrome c oxidase subunit II interaction. Exp. Cell Res. *317*, 1608–1620.

Principe, D.R., Diaz, A.M., Torres, C., Mangan, R.J., DeCant, B., McKinney, R., Tsao, M.S., Lowy, A., Munshi, H.G., Jung, B., et al. (2017). TGFbeta engages MEK/ERK to differentially regulate benign and malignant pancreas cell function. Oncogene *36*, 4336–4348.

Prunier, C., Baker, D., Ten Dijke, P., and Ritsma, L. (2019). TGF-beta family signaling pathways in cellular dormancy. Trends Cancer *5*, 66–78.

Reinke, H., and Asher, G. (2019). Crosstalk between metabolism and circadian clocks. Nat. Rev. Mol. Cell Biol. *20*, 227–241.

Relles, D., Sendecki, J., Chipitsyna, G., Hyslop, T., Yeo, C.J., and Arafat, H.A. (2013). Circadian gene expression and clinicopathologic correlates in pancreatic cancer. J. Gastrointest. Surg. *17*, 443–450.

Relogio, A., Thomas, P., Medina-Perez, P., Reischl, S., Bervoets, S., Gloc, E., Riemer, P., Mang-Fatehi, S., Maier, B., Schafer, R., et al. (2014). Ras-mediated deregulation of the circadian clock in cancer. PLoS Genet. *10*, e1004338.

Satelli, A., and Li, S. (2011). Vimentin in cancer and its potential as a molecular target for cancer therapy. Cell. Mol. Life Sci. *68*, 3033–3046.

Sato, F., Bhawal, U.K., Yoshimura, T., and Muragaki, Y. (2016). DEC1 and DEC2 crosstalk between circadian rhythm and tumor progression. J. Cancer *7*, 153–159.

Sato, F., Kohsaka, A., Takahashi, K., Otao, S., Kitada, Y., Iwasaki, Y., and Muragaki, Y. (2017). Smad3 and Bmal1 regulate p21 and S100A4 expression in myocardial stromal fibroblasts via TNF-alpha. Histochem. Cell Biol. *148*, 617–624.

Sato, F., Otsuka, T., Kohsaka, A., Le, H.T., Bhawal, U.K., and Muragaki, Y. (2019). Smad3 suppresses epithelial cell migration and proliferation via the clock gene Dec1, which negatively regulates the expression of clock genes Dec2 and Per1. Am. J. Pathol. *189*, 773–783.

Scandura, J.M., Boccuni, P., Massague, J., and Nimer, S.D. (2004). Transforming growth factor beta-induced cell cycle arrest of human hematopoietic cells requires p57KIP2 up-regulation. Proc. Natl. Acad. Sci. U S A *101*, 15231–15236.

Schutte, M., Hruban, R.H., Hedrick, L., Cho, K.R., Nadasdy, G.M., Weinstein, C.L., Bova, G.S., Isaacs, W.B., Cairns, P., Nawroz, H., et al. (1996). DPC4 gene in various tumor types. Cancer Res. *56*, 2527–2530.

Shin, S.H., Kim, H.J., Hwang, D.W., Lee, J.H., Song, K.B., Jun, E., Shim, I.K., Hong, S.M., Kim, H.J., Park, K.M., et al. (2017). The DPC4/SMAD4 genetic status determines recurrence patterns and treatment outcomes in resected pancreatic ductal adenocarcinoma: a prospective cohort study. Oncotarget *8*, 17945–17959.

Siegel, P.M., and Massague, J. (2003). Cytostatic and apoptotic actions of TGF-beta in homeostasis and cancer. Nat. Rev. Cancer *3*, 807–821.

Singh, P., Srinivasan, R., and Wig, J.D. (2012). SMAD4 genetic alterations predict a worse prognosis in patients with pancreatic ductal adenocarcinoma. Pancreas *41*, 541–546.

Sulli, G., Lam, M.T.Y., and Panda, S. (2019). Interplay between circadian clock and cancer: new frontiers for cancer treatment. Trends Cancer *5*, 475–494.

Sulli, G., Rommel, A., Wang, X., Kolar, M.J., Puca, F., Saghatelian, A., Plikus, M.V., Verma, I.M., and Panda, S. (2018). Pharmacological activation of REV-ERBs is lethal in cancer and oncogene-induced senescence. Nature *553*, 351–355.

Sun, C., Yamato, T., Furukawa, T., Ohnishi, Y., Kijima, H., and Horii, A. (2001). Characterization of the mutations of the K-ras, p53, p16, and SMAD4 genes in 15 human pancreatic cancer cell lines. Oncol. Rep. *8*, 89–92.

Tabu, K., Kimura, T., Sasai, K., Wang, L., Bizen, N., Nishihara, H., Taga, T., and Tanaka, S. (2010). Analysis of an alternative human CD133 promoter reveals the implication of Ras/ERK pathway in tumor stem-like hallmarks. Mol. Cancer *9*, 39.

Takano, S., Kanai, F., Jazag, A., Ijichi, H., Yao, J., Ogawa, H., Enomoto, N., Omata, M., and Nakao, A. (2007). Smad4 is essential for down-regulation of E-cadherin induced by TGF-beta in pancreatic cancer cell line PANC-1. J. Biochem. *141*, 345–351.

Tavano, F., Pazienza, V., Fontana, A., Burbaci, F.P., Panebianco, C., Saracino, C., Lombardi, L., De Bonis, A., di Mola, F.F., di Sebastiano, P., et al. (2015). SIRT1 and circadian gene expression in pancreatic ductal adenocarcinoma: effect of starvation. Chronobiol. Int. *32*, 497–512.

Voss, M., Wolff, B., Savitskaia, N., Ungefroren, H., Deppert, W., Schmiegel, W., Kalthoff, H., and Naumann, M. (1999). TGFbeta-induced growth inhibition involves cell cycle inhibitor p21 and pRb independent from p15 expression. Int. J. Oncol. *14*, 93–101.

Wang, F., Li, C., Yongluo, and Chen, L. (2016). The circadian gene clock plays an important role in cell apoptosis and the DNA damage response in vitro. Technol. Cancer Res. Treat. *15*, 480–486.

Watanabe, M., Sheriff, S., Lewis, K.B., Cho, J., Tinch, S.L., Balasubramaniam, A., and Kennedy, M.A. (2012). Metabolic profiling comparison of human pancreatic ductal epithelial cells and three pancreatic cancer cell lines using NMR based metabonomics. J. Mol. Biomark. Diagn. *3*, S3-S002.

Wheelock, M.J., Shintani, Y., Maeda, M., Fukumoto, Y., and Johnson, K.R. (2008). Cadherin switching. J. Cell Sci. *121*, 727–735.

Wu, Y., Sato, F., Yamada, T., Bhawal, U.K., Kawamoto, T., Fujimoto, K., Noshiro, M., Seino, H., Morohashi, S., Hakamada, K., et al. (2012). The BHLH transcription factor DEC1 plays an important role in the epithelial-mesenchymal transition of pancreatic cancer. Int. J. Oncol. *41*, 1337–1346.

Xu, J., Lamouille, S., and Derynck, R. (2009). TGF-beta-induced epithelial to mesenchymal transition. Cell Res. *19*, 156–172.

Yalcin, M., El-Athman, R., Ouk, K., Priller, J., and Relogio, A. (2020). Analysis of the circadian regulation of cancer hallmarks by a cross-platform study of colorectal cancer time-series data reveals an association with genes involved in huntington's disease. Cancers (Basel) *12*, 963.

Yamada, S., Fujii, T., Shimoyama, Y., Kanda, M., Nakayama, G., Sugimoto, H., Koike, M., Nomoto, S., Fujiwara, M., Nakao, A., et al. (2015). SMAD4 expression predicts local spread and treatment failure in resected pancreatic cancer. Pancreas *44*, 660–664.

Yang, J., Antin, P., Berx, G., Blanpain, C., Brabletz, T., Bronner, M., Campbell, K., Cano, A., Casanova, J., Christofori, G., et al. (2020). Guidelines and definitions for research on epithelial-mesenchymal transition. Nat. Rev. Mol. Cell Biol. *21*, 341–352.

Yao, D., Dai, C., and Peng, S. (2011). Mechanism of the mesenchymal-epithelial transition and its relationship with metastatic tumor formation. Mol. Cancer Res. *9*, 1608–1620.

Zawel, L., Yu, J., Torrance, C.J., Markowitz, S., Kinzler, K.W., Vogelstein, B., and Zhou, S. (2002). DEC1 is a downstream target of TGF-beta with sequence-specific transcriptional repressor activities. Proc. Natl. Acad. Sci. U S A *99*, 2848–2853.

Zhang, Y.E. (2017). Non-smad signaling pathways of the TGF-beta family. Cold Spring Harb. Perspect. Biol. *9*, a022129.

iScience, Volume *23*

Supplemental Information

Circadian Dysregulation of the TGFβ/SMAD4 Pathway Modulates Metastatic Properties and Cell Fate Decisions in Pancreatic Cancer Cells

Yin Li, Alireza Basti, Müge Yalçin, and Angela Relógio

Supplemental Data Items

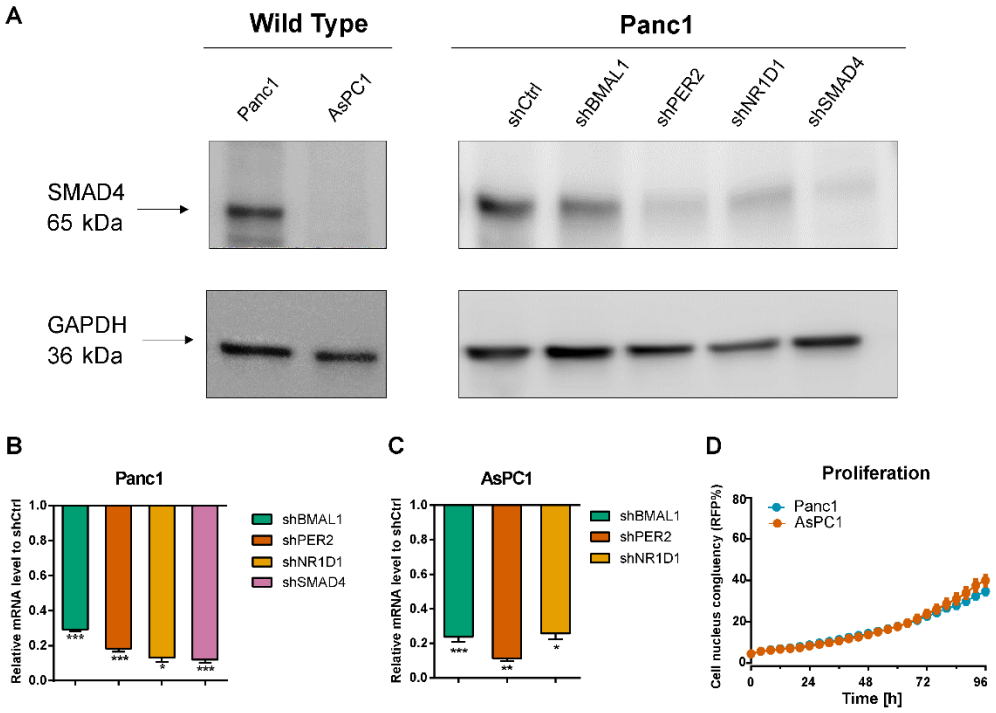

Figure S1. Western blot analysis of SMAD4 protein expression for KDs and OE cells. Related to Figure 1. (A) Western blot analysis of SMAD4 (65kDa) for wild type PDA cells and Panc1 KD cells (*shCtrl*, *shBMAL1*, *shPER2*, *shNR1D1* and *shSMAD4*). Depicted is one representative replicate, GAPDH is provided as loading control. (B - C) KD efficiency for sh*BMAL1*, sh*PER2*, sh*NR1D1* and sh*SMAD4*. Gene expression analysis of corresponding KD genes in Panc1 (B) and AsPC1 (C) cells. Relative gene expression is shown compared to the corresponding *shCtrl* (pLKO.1) (mean ± SEM, n = 3, t-test, **p* < 0.05, ***p* < 0.01, ****p* < 0.001). KD efficiency in Panc1 *shBMAL1*: 70.8% (0.29 ± 0.01), *shPER2*: 81.7% (0.18 ± 0.02), *shNR1D1*: 86.1% (0.13 ± 0.02) and *shSMAD4*: 88.5% (0.12 ± 0.02). KD efficiency in AsPC1 *shBMAL1*: 76.2% (0.24 ± 0.03), *shPER2*: 88.7% (0.11 ± 0.02) and *shNR1D1*: 74.2% (0.26 ± 0.03). (D) Proliferation assays for pancreatic cell lines (Panc1 and AsPC1) were performed using NucLight Rapid Red Reagent for the IncuCyte S3 Live Cell System Analysis (mean ± SEM, n = 8).

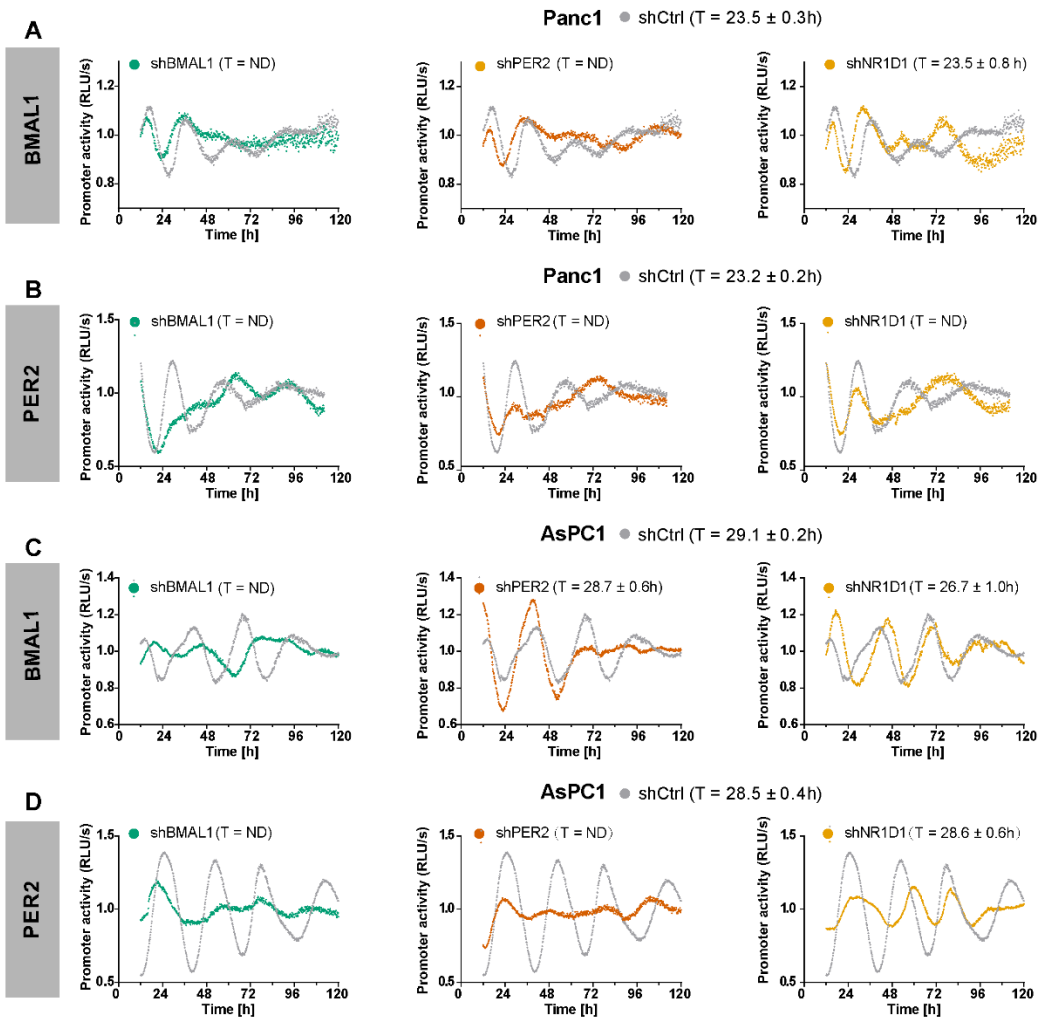

Figure S2. The promoter activity of BMAL1 and PER2 after clock genes KD. Related to Figure 2. Bioluminescence recordings for the promoter activity of *BMAL1* and *PER2* for *shCtrl* (pLKO.1) and KDs (*shBMAL1*, *shPER2* and *shNR1D1)* in Panc1 (A - B) and AsPC1 (C - D). Depicted is one representative replicate (mean ± SEM, n = 3).

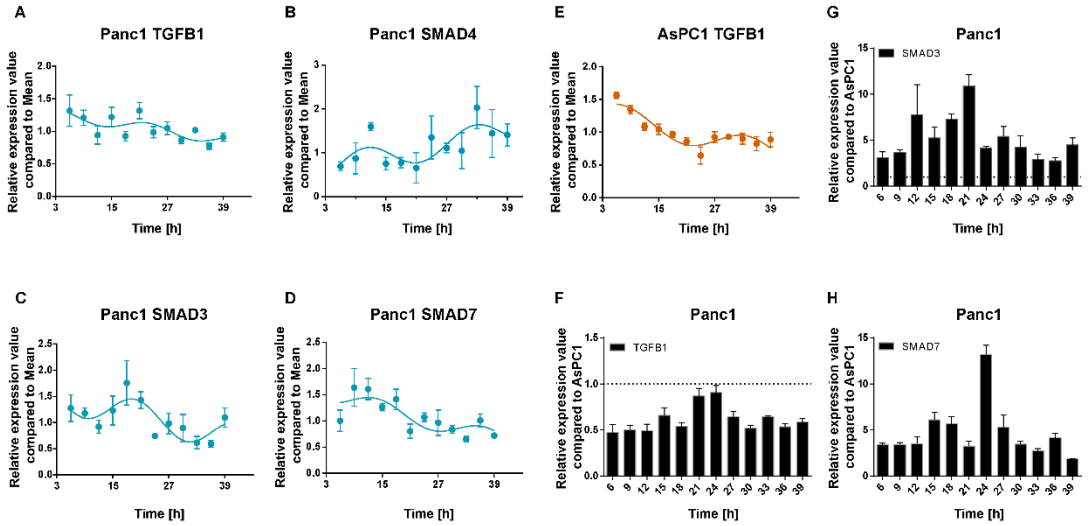

Figure S3. Panc1 (SMAD4 proficient) cells show circadian oscillations in expression for elements of the TGFβ pathway. Related to Figure 2. (A - E) 33h time-course gene expression analysis for *TGFβ1*, *SMAD4*, *SMAD3* and *SMAD7* in Panc1 and AsPC1 wild type cells (n = 3, mean ± SEM, a cosine curve was fitted to all data sets, Table. 3). (F - H) Comparisons of gene expression (*SMAD3*, *SMAD7* and *TGFβ1*) for each time point over 33 h (mean ± SEM, n = 3).

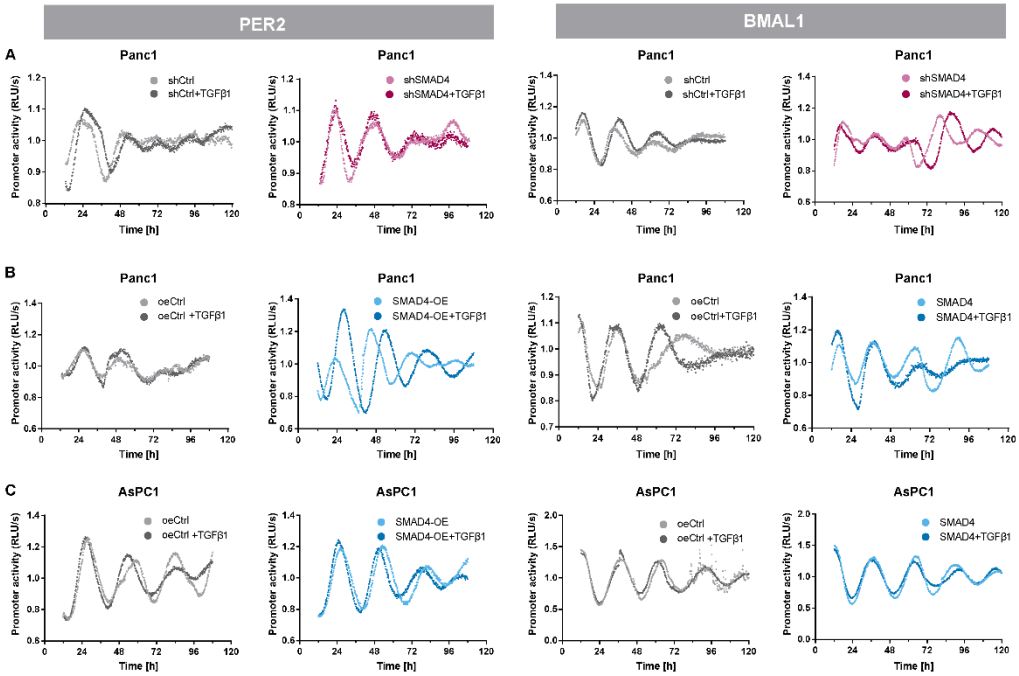

Figure S4. The real-time bioluminescence recording of a *BMAL1* and *PER2* promoter activity for activation or inactivation of the canonical TGFβ pathway. Related to Figure 2.

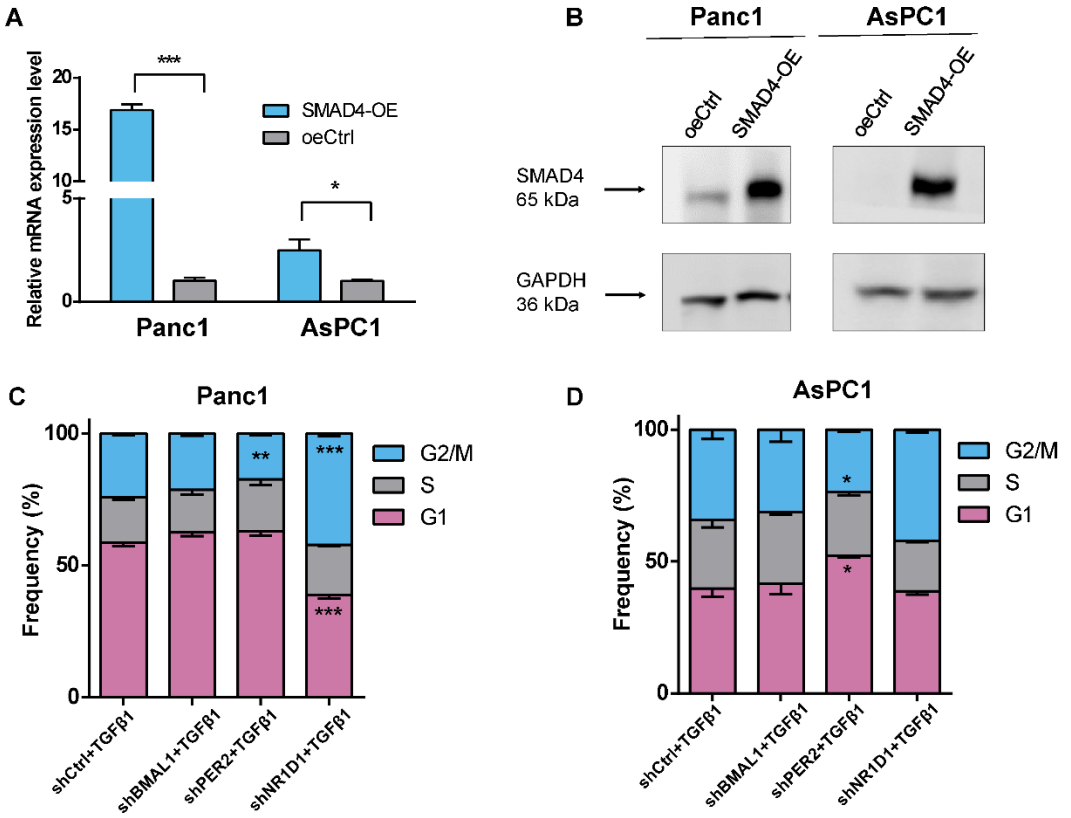

Figure S5. Clock disruption stimulated with TGFβ impacts on cell cycle in PDA cells. Related to Figures 3 and 4. (A) *SMAD4* overexpressing efficiency after γ-retroviruses transduction. Gene expression analysis of *SMAD4* in Panc1 and AsPC1 cells. Relative gene expression value is shown compared to the corresponding empty vector oeCtrl (Flag-puro). (B) Shown is one representative replicate for the Western blot analysis of SMAD4 (65kDa) for PDA cells containing overexpression construct and respective control (*SMAD4*-OE and oeCtrl). GAPDH was d as loading control. (mean ± SEM, n = 3). (C-D) Cell cycle measurements after KDs of BMAL1, PER2 and NR1D1 with or without a 24h-TGFβ1 stimulation. Cell cycle phase distributions were compared with their respective control conditions (n = 3, mean ± SEM, two-way ANOVA, *$p < 0.05$, **$p < 0.01$, ***$p < 0.001$).

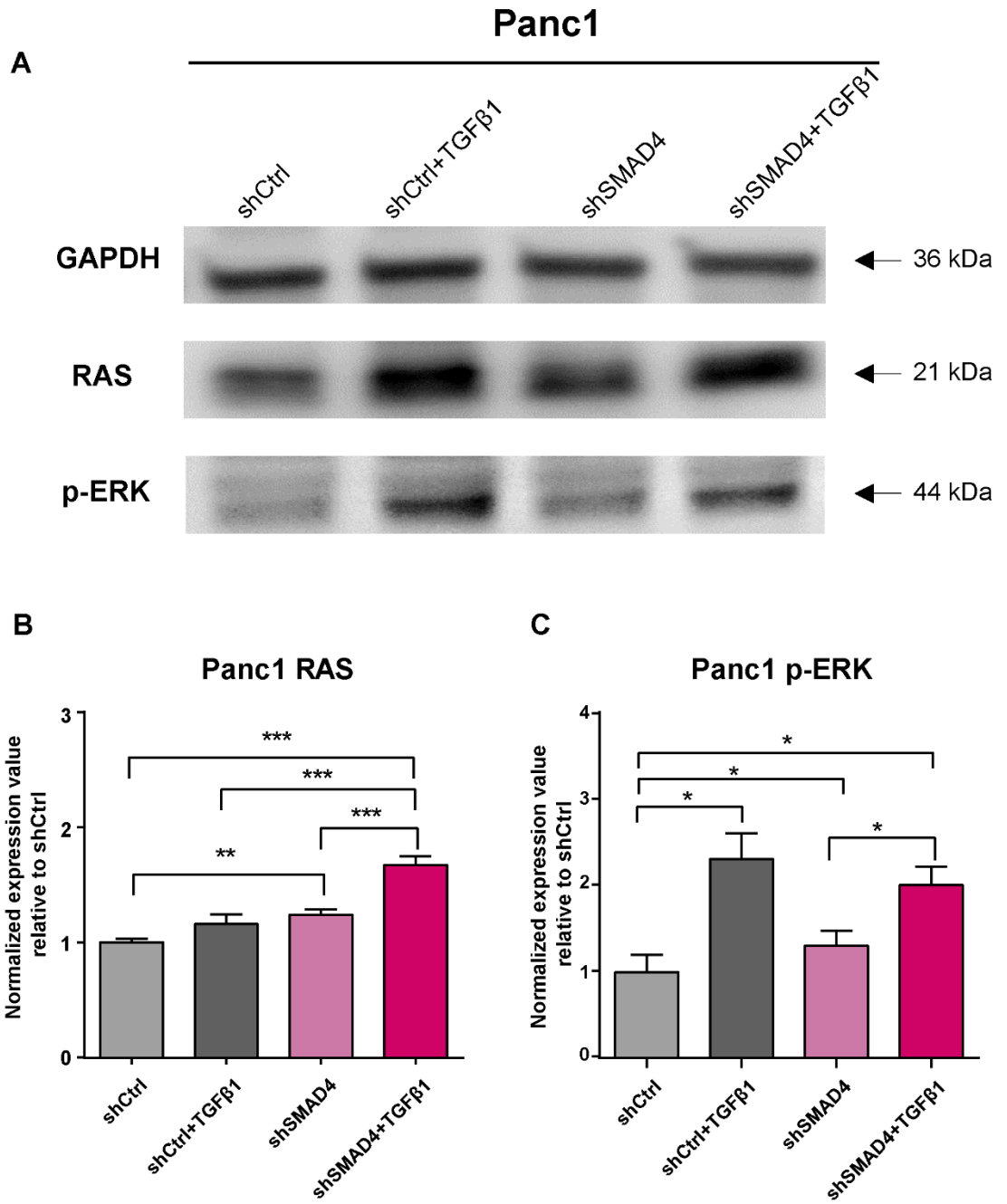

Figure S6. Loss of SMAD4 and TGFβ stimulation promote the overexpression of p-ERK and RAS. Related to Figures 3 and 4. (A) Shown is one representative replicate for the Western blot analysis of RAS (21kDa) and phosphorylated-ERK (p-ERK, 44.42kDa) for Panc1 cells containing *shSMAD4* construct and respective control (*SMAD4*-KD and *shCtrl*) with or without a 24h-TGFβ-stimulation. GAPDH (36kDa) was used as loading control. (B-C) Relative protein expression level of RAS, p-ERK for each condition as compared to *shCtrl* (one-way ANOVA, mean ± SEM, n ≥ 3, **p* < 0.05, ***p* < 0.01, ****p* < 0.001).

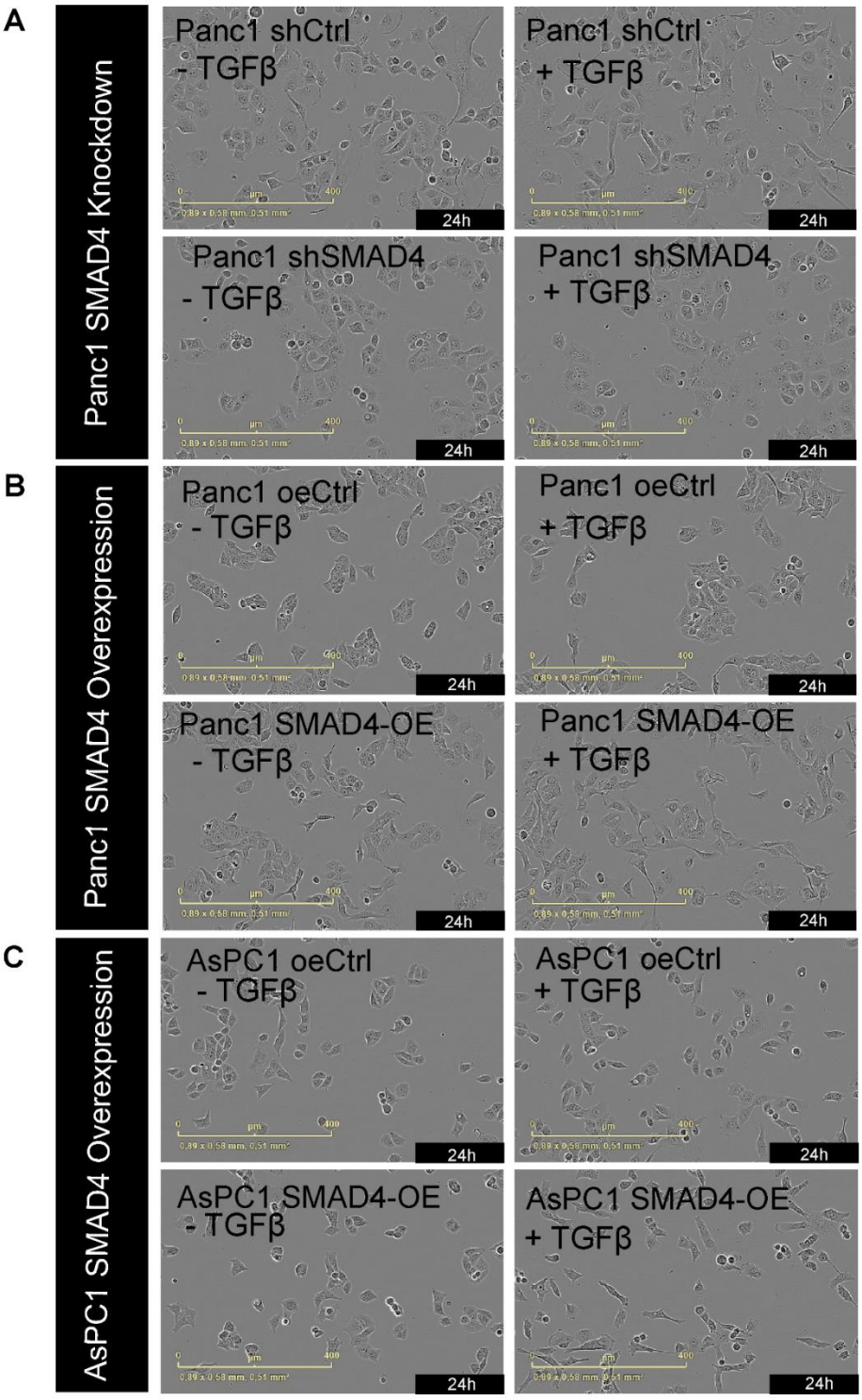

Figure S7. Morphology changes after activation and inactivation of the canonical TGFβ pathway. Related to Figure 5. *SMAD4*-KD and -OE cells were stimulated with 10ng/ml TGFβ1 or the corresponding solvent. Changes in cell morphology were observed 24h after stimulation (20x objective, scale bar = 400 µm).

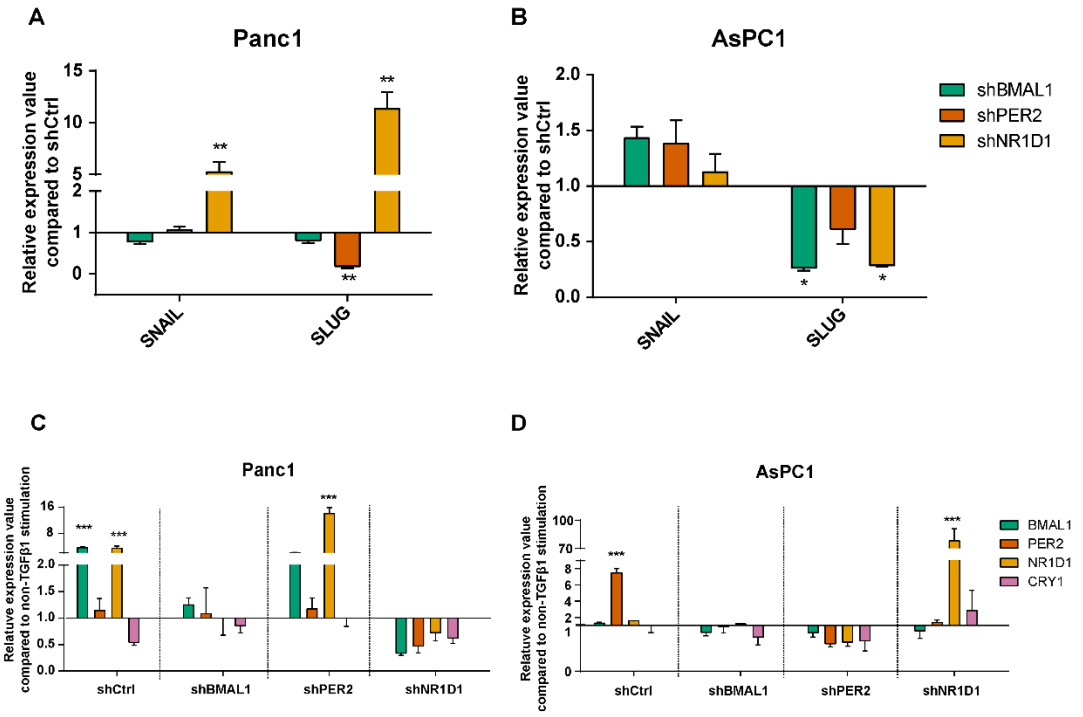

Figure S8. TGFβ stimulation impacts the clock gene expression differentially in SMAD4-proficient and -deficient PDA cells. Related to Figure 6. (A - B) mRNA levels of EMT markers (*SNAIL and SLUG*) in PDA cells were altered after knockdown of core-clock genes (*shBMAL1*, *shPER2* and *shNR1D1*). Depicted are RT-qPCR results for KD PDA cells compared to the *shCtrl* (mean ± SEM, n = 3, t-test, **p* < 0.05, ***p* < 0.01, ****p* < 0.001). (C - D) The comparison of clock genes (*BMAL1*, *PER2*, *NR1D1* and *CRY1*) expression with stimulation of TGFβ1 (10ng/ml) or its solvent. Data shown as comparison to the non-TGFβ1 stimulation (mean ± SEM, n = 3, t-test **p* < 0.05, ***p* < 0.01, ****p* < 0.001).

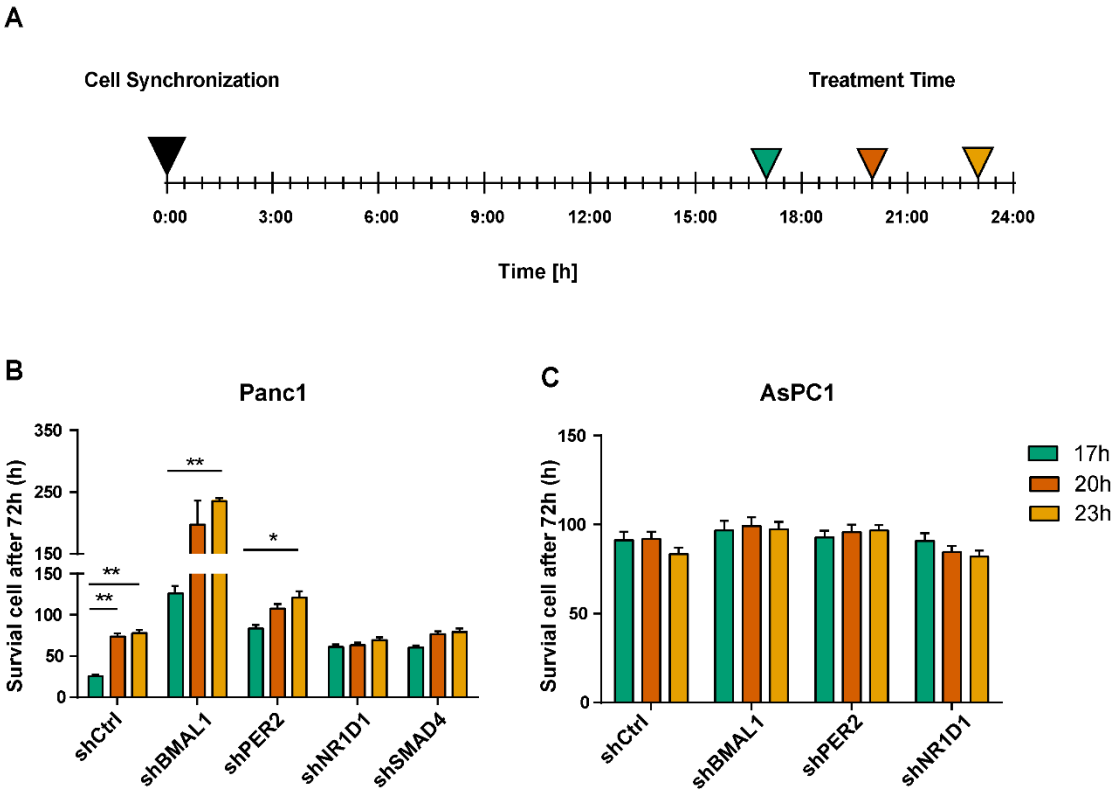

Figure S9. Cytotoxicity assays were performed using NucLight Rapid Red Reagent for the IncuCyte S3 Live Cell System Analysis. Related to Figure 7. (A) At 17h, 20h, 23h after cell synchronization respectively, gemcitabine was added to the cell culture medium. (B - C) 72h after treatment, the number of living cells per well was quantified using the IncuCyte S3 Live-Cell Analysis System. Depicted are the comparisons to the 17h time point. (means ± SEM, n = 6, two-way ANOVA, *$p < 0.05$, **$p < 0.01$, ***$p < 0.001$).

Table S1. Primer sequences.

	Primer sequence	
Gene	**Forward**	**Reverse**
SMAD3	F:5'-CCCCAGAGCAATATTCCAGA-3'	R:5'-GGCTCGCAGTAGGTAACTGG-3'
SMAD4	F:5'-TGTGCCTGGTTTGATGGTAA-3'	R:5'-GCCATTTTCCCAATCTGCTA-3'
SMAD7	F:5'-TACCGTGCAGATCAGCTTTG-3'	R:5'-AGTTTGAAGTGTGGCCTGCT-3'
DEC1	F:5′-GTCTGTGAGTCACTCTTCAG-3	R:5′-GAGTCTAGTTCTGTTTGAAGG-3′
DEC2	F:5′-CACCTTTGACGTCTTTGGAG-3′	R:5′-GAGAGTGGGAATAGATGCAC-3′
E-cadherin	F:5'-ATTGCAAATTCCTGCCATTC-3'	R:5'-CTCTTCTCCGCCTCCTTCTT-3'
N-cadherin	F:5'-CTCCTATGAGTGGAACAGGAACG-3′	R:5'-TTGGATCAATGTCATAATCAAGTGCTGTA-3'
Vimentin	F:5'-GGGAGAAATTGCAGGAGGAG-3'	R:5'-ATTCCACTTTGCGTTCAAGG-3'
CD133	F:5'-CCCCAGGAAATTTGAGGAAC-3'	R:5'-TCCAACAATCCATTCCCTGT-3'
SNAIL	F: 5′-GAGGCGGTGGCAGACTAG-3′	R: 5′-GACACATCGGTCAGACCAG-3′
SLUG	F: 5′-CATGCCTGTCATACCACAAC-3′	R: 5′-GGTGTCAGATGGAGGAGGG-3′

Transparent Methods

Cell culture

The PDA cell lines Panc1 and AsPC1 were used as an *in vitro* model system for our study. Panc1 (ATCC: CRL-1469) was derived from the primary tumor of a male patient with a doubling time of 52h (Lieber et al., 1975). AsPC1 (ATCC: CRL-1682) was established from ascites of a female patient with similar doubling time as Panc1 (Watanabe et al., 2012). Both cell lines were maintained in RPMI 1640 (Gibco, CA, USA) supplemented with 1% penicillin-streptomycin (Gibco) and 10% fetal bovine serum (Gibco). For lumicycle measurements and IncuCyte S3 analysis, RPMI 1640 (Gibco) was supplemented with 10µM HEPEs (Gibco) to avoid pH variation. All cells were incubated at 37°C in a humidified atmosphere with 5% CO2.

Lentivirus production of *Bmal1*: Luc, *Per2*: Luc reporters and shRNA-mediated knockdown

Lentiviral elements containing a *BMAL1*-promoter-driven luciferase (BLH) or a *PER2*-promoter-driven-Luciferase (PLB) were generated as previously described (Brown et al., 2005). For the knockdown of *BMAL1*, *PER2*, *NR1D1* and *SMAD4*, a TRC lentiviral shRNA glycerol set (Dharmacon Inc., Lafayette, CO, USA) specific for each gene was used consisting of 5 - 6 individual shRNAs. The construct with best knockdown efficiency was determined by RT-qPCR or Western-blot analysis and used for further experiments.

For lentiviral production, HEK293T (ATCC: CRL-11268) cells were seeded in a 75 cm^2 cell culture flask and co-transfected with 4.2 µg packaging plasmid psPAX, 2.5 µg envelope plasmid pMD2G and 5.8 µg expression plasmid (Bmal1:luc-hygromycin, PER2:luc-Blasticidin, pLKO.1 empty vector or specific knockdown plasmids) using the CalPhos mammalian transfection kit (Clontech Fremont, CA, USA) according to the manufacturer's instruction. Virus particles were harvested and centrifuged at 4000xg for 15 min to remove cell debris. The supernatant was filtered (0.45 µm filter, Sarstedt, Nümbrecht, DE) and used for lentiviral transduction.

Retrovirus production for *SMAD4* overexpression

pBabe-puro-Smad4-Flag was a gift from Sam Thiagalingam (Addgene plasmid # 37041; http://n2t.net/addgene:37041; RRID: Addgene_37041). To generate retrovirus, HEK293T (human, kidney, ATCC: CRL-11268) cells were seeded in 75 cm^2 culture flasks and co-transfected by 6µg pBabe-puro empty vector or pBabe-Smad4-Flag along with 0.3 µg PMD2.G envelope and 2.7µg pUMVC packaging plasmids using FuGENE HD Transfection Reagent (Promega, WI, USA) according to manufacturer's introduction. The supernatant was replaced after 12 h, subsequently, retroviral particles were collected at 24h and 36h after incubation. The retroviral particles were centrifuged at 4100xg for 15 min to remove cell debris filtered (45 µm filter, Sarstedt, Nümbrecht, DE), and stored at -80°C for further usage.

Lentivirus and retrovirus transduction

Cells were transduced with 1.5 ml virus filtrate including 8 µg/µl protamine sulphate (Sigma, MO, USA) and 4 µg/µl polybrene (Sigma) in 6-well plates. To enhance transduction efficiency, plates were centrifuged at 800xg for 90 minutes at 35°C. Subsequently, the supernatant was replaced after 6 - 8 hours. Stably-transduced cells were selected using the corresponding antibiotics (BMAL1: Luc hygromycin, PER2: Luc blasticidin; *shBMAL1*, *shPER2*, *shNR1D1*, *shSMAD4* and pLKO.1 empty vector puromycin; pBabe-puro empty vector and pBabe-Smad4-Flag puromycin). Untraduced cells were used as control. pLKO.1 empty vector and pBabe-puro empty vector are referred as *shCtrl* and oeCtrl respectively.

Cell synchronisation

For all experiments, cells were synchronized by medium change. For the cytotoxicity analysis, time point 0 h is defined as the time point of medium change. Untreated control cells were prepared in the same way, but treated with the corresponding vehicle control (H2O for gemcitabine).

Bioluminescence measurement

For live-cell bioluminescence measurements, cells were seeded onto 35mm dishes (Thermo scientific MA, USA) and maintained in phenol red-free RPMI1640 (Gibco) containing 10% FBS, 1% penicillin-streptomycin, 10µM HEPES supplemented with 250 µM D-Luciferin (PJK, Kleinblittersdorf, DE). Prior to the measurement, cells were synchronized by medium change and washed with 1xPBS twice to avoid the influence of phenol red. Subsequently, the live-cell bioluminescence was recorded by a LumiCycle instrument (Actimetrics, Wilmette, IL, USA) for five consecutive days. For live-cell bioluminescence measurements of *SMAD4* knockdown or overexpression with TGFβ1 stimulation, cells were treated and maintained with 10ng/ml TGFβ1 (Stem Cell Technologies, Vancouver, CA) for five consecutive days. The concentration of TGFβ1 was retrieved from a previous publication (Ellenrieder et al., 2001). Chronostar software was used for data analysis (Sporl et al., 2011). The data of the first 12 hours was automatically excluded to avoid the influence of intrinsic noise of the device. Bioluminescence measurements were performed at least three times, as indicated.

RNA extraction and gene expression analysis by RT-qPCR

Total RNA was isolated with the plus RNeasy Mini kit (Qiagen, Venlo, NL) following the manufacturer's instructions. For a single time-point RT-qPCR, cell medium was replaced by fresh medium 3 hours before RNA extraction. Subsequently, the medium was discarded and cell pellets were washed twice with 1xPBS. To digest genomic DNA, homogenized cell lysates were passed through gDNA eliminator spin column with a 30s centrifugation at 17000xg. RNA was eluted in 20-30 µl Rnase-free water. The final RNA concentration was measured using a Nanodrop 1000 (Thermo Fisher Scientific) and stored at -80 °C for further usage. For RT-qPCR analysis, the extracted RNA was reverse transcribed into cDNA by using random hexamers

(Eurofins MWG Operon) and Reverse Transcriptase (Life technologies). RT-qPCR was performed using SsoAdvanced Universal SYBR Green Supermix (Bio-Rad Laboratories, Hercules, CA, USA) in 96-well plates. For the detection of human gene expression, primers were either custom designed (**Table. S1**) or a human Quantitect Primer assay (Qiagen) was used. Gene expression levels were normalised by Gapdh mRNA. The qPCR was performed in a CFX Connect Real-Time PCR Detection System (Biorad). Relative gene expression was calculated using the $2^{-\Delta\Delta Ct}$ method (Livak and Schmittgen, 2001). Mean and SEM were calculated including biological and technical replicates.

Proliferation assays

For the proliferation assay, 5000 cells/ well of each condition were seeded in a 96-well plate (Sarstedt). Cells were allowed to adhere. Subsequently, the medium was replaced with fresh medium containing TGFβ1 or its solvent. Plates were measured in the IncuCyte® S3 Live Cell System Analysis (Sartorius, Göttingen, Germany). Four images per well were recorded every 2 hours. The analysis was performed using the IncuCyte S3 Software (Sartorius).

For TGFβ1 stimulation, stimulated and control cells were treated with and maintained in 10ng/ml TGFβ1 (Stem Cell Technologies, Vancouver, CA) or its solvent (0.1% BSA, Sigma) for five consecutive days.

Apoptosis assays

Cells were seeded in a 96-well plate (Sarstedt) at a concentration of 5000 cells/ 100 µL RPMI medium and incubated overnight at 37 °C with 5% CO2. After incubation, cell media were replaced with fresh medium containing caspase 3/7 reagent (Sartorius, 1:2000) and TGFβ1 or its solvent. Cell apoptosis was measured using the IncuCyte® S3 Live Cell System Analysis (Sartorius). Cells were scanned every 2 hours with a 20x objective and by using the phase and green image channels.

Migration assays

60000 cells/ well of each condition were seeded in a 96-well Essen Image Lock TM microplate (Essen BioScience, Michigan, USA) and incubated overnight at 37 °C, 5% CO2. In the next day, the WoundMakerTM (Essen BioScience) was used to create precise and reproducible wounds. Subsequently, the medium was replaced with a fresh medium containing TGFβ1 (10 ng/mL) or its solvent and the plate was placed in the IncuCyte® S3 Live Cell System Analysis (Essen BioScience). Image acquisition was performed by setting the “scan type” to Scratch Wound and Wide Mode, using the 10x objective. The plate was scanned every 2 hours. The analysis was performed in the IncuCyte S3 Software (Sartorius), the wound width for each well were exported and the migration speed were calculated using either the time of wound closed or the cut-off of 48 hours, which is shorter than the doubling-times of Panc1 and AsPC1 (48 - 52h). Biological triplicates and 8 technical replicates were carried out for each experiment.

Invasion assays

5000 cells/ well of each condition were mixed with 20µl 5mg/ml Basement Membrane Matrix (Trevigen Gaithersburg, MD, USA) seeded in the inner chamber of a 96-well Incucyte Chemotaxis cell invasion clear view plates (Sartorius). Subsequently, the plate was centrifuged at 50x G to avoid the formation of bubbles. Basement membrane matrix was allowed to polymerize at 37°C for 45 minutes to form a reconstituted basement membrane. Cell invasion was measured using the IncuCyte® S3 Live Cell System Analysis. Cells were scanned every 2 h with a 20x objective and phase image channels. Biological triplicates and 8 technical replicates were carried out for each experiment.

Cytotoxicity assays

5000 cells/well were seeded in a 96-well plate (Sarstedt) containing 100 µL RPMI medium and incubated overnight at 37 °C with 5% CO2. After incubation, the supernatant was replaced with fresh medium containing IncuCyte® Cytotox Reagents (Sartorius, (Red)) and appropriate concentrations of gemcitabine (Panc1, 9.5µM; AsPC1, 23.9µM (Awasthi et al., 2013)). For the time-dependent treatment assay, cells were synchronized by a medium change. At specific time points after synchronization (17h, 20h and 23h). Gemcitabine in a solution containing IncuCyte® Cytotox Reagents (Red) was added into each well with a micro-pipette. Cell cytotoxicity was measured using the IncuCyte® S3 Live Cell System Analysis (Sartorius). Cells were scanned every 2 hours with a 20x objective and using the phase and red image channels. Biological triplicates and 8 technical replicates were carried out for each experiment.

Cytotoxicity assays with live-cell nuclear labelling

Cells were labelled with IncuCyte® NucLight Rapid Red Reagent (Sartorius) 30 min before measurements. Cell survival after treatment was quantified using the IncuCyte® S3 Live Cell System Analysis (Sartorius). The plates were scanned every 2 hours with a 20x objective and using the phase and red image channels.

Treatment with Gemcitabine

Treatment concentrations for each PDA cell line were determined based on the experimentally determined IC50 value in a previous study (Awasthi et al., 2013).

Western blot

Cells were synchronized by medium change, gently detached from the dish at 3h after synchronization, sedimented by low-speed centrifugation and resuspended in lysis buffer. Aliquots containing 20 mg of proteins from each cell lysate were subjected to SDS polyacrylamide gel electrophoresis and transferred to a Nitrocellulose Membranes (GE Healthcare Amersham™) using Trans-Blot Turbo Transfer System. Membranes were probed with the following primary antibodies: SMAD4 (1:5000; ab40759, Abcam, Cambridge, UK); GAPDH (1:20000; ab9485, Abcam); RAS (1:5000; ab52939, Abcam); p-ERK (1:2000, Cell

Signaling Technology, Frankfurt am Main, Germany). After incubation with corresponding secondary antibody (1:2000; ab205718, Abcam), signals were detected using the Amersham ECL Select Western Blotting Detection Reagent (GE Health care, Chicago, US), acquired by Image Quant LAS 4000 series (GE Health care). Data was analysed by image J v1.8 (developed by National Institutes of Health).

Cell cycle analysis

$1x10^6$ cells under the logarithmic growth phase were collected, washed with 1xPBS (Gibco) and fixed with ice cold 80% ethanol. Cells were maintained in medium containing 10ng/ml TGFβ1 stimulation (or the solvent) for 24 hours before the measurement. Subsequently, samples were washed with PBS and incubated in a 200ul of 1xPBS solution containing 0.5% Tween20 (Sigma), 1% BSA (Sigma), 2 N HCl/Triton x-100 (Sigma) and 10 mg/mL of Rnase (AppliChem, Cat. No. A2760) for 30 minutes at room temperature. For PI staining, supernatant was removed, the fixed cell pellets were resuspended and stained in 500 µL of 1xPBS containing 50 µM PI (Sigma) for 30 minutes at 37°C. Subsequently, supernatant containing PI solution was removed and the stained cells were resuspended in cold 500 µL 1xPBS and read in FACS Cabilur (Becton Dickinson, NJ, USA). Cell cycle analysis was conducted by fitting a univariate cell cycle model using the Watson pragmatic algorithm as implemented in FlowJo v10.2 (FlowJo LLC).

Statistical Analysis

Experiments were carried out with at least three biological replicates per condition. Data are provided as mean ± SEM. *p*-value < 0.05 was considered as statistically significant. The significance of differences between groups (*$p < 0.05$; **$p < 0.01$; ***$p < 0.001$) was analysed by one-way or two-way ANOVA followed by Tukey`s multiple comparisons test and the unpaired two-tailed t-test or multiple t-tests using the Prism software (version 6.0; GraphPad Prism).

Cosinor Analysis

To detect significant ($p < 0.05$) circadian rhythmic expression, the cosinor analysis was performed. The *p*-value was calculated using a QUICK CALCS (GraphPad, https://www.graphpad.com/quickcalcs/pValue1/). The oscillating transcripts were estimated by GrapdPad Prism. 6 software and fitting a non-linear equation as following:

$$Y(t) = B + A \cdot (\cos\frac{2\pi \cdot t}{P} + \varphi) + S \cdot t$$

t = Time, B = baseline, A = amplitude, S = slope, φ = acrophase, P = period.

Analysis of pancreatic adenocarcinoma data from a cohort of patients retrieved from the TCGA data base

Clinical information for pancreatic adenocarcinoma with overall patient survival was retrieved from The Cancer Genome Atlas (TCGA) (https://portal.gdc.cancer.gov). Mutational frequencies in the TCGA PDA patient population (184 pancreatic adenocarcinoma samples from PanCancer Atlas) were plotted using cBio Cancer Genomics Portal (http://cbioportal.org) (Cerami et al., 2012; Gao et al., 2013). OncoPrint functionality was used for graphical representation of mutation frequency for 10 candidate genes retrieved from our results. Survival curves were plotted using a Cox model that includes coxph (Surv (times, died) ~ gene + grade1 + grade2 + grade3 + age) via OncoLnc (http://www.oncolnc.org), each tumour grade is represented as a separate term as 1 or 0 (Anaya, 2016). The survival data includes clinical data for patients with complete clinical information needed for the analysis and based on a follow up or days until death greater than zero. Previous studies revealed contribution of additional clinical parameters to the benefit provided by chronotherapy (i.e., age). Therefore, in our cox survival analysis we included patient age as an additional clinical parameter. The PDA cohort was divided into two equal groups (N1=87, N2=87 patients). based on the mean expression value of the candidate gene, the change in gene expression levels were categorized as high or low for equal number of patients in the cohort (N = 87 for high expression group and N = 87 for low expression group).

Supplemental References

Anaya, J. (2016). OncoLnc: Linking TCGA survival data to mRNAs, miRNAs, and lncRNAs (PeerJ Preprints).

Awasthi, N., Zhang, C., Schwarz, A.M., Hinz, S., Wang, C., Williams, N.S., Schwarz, M.A., and Schwarz, R.E. (2013). Comparative benefits of Nab-paclitaxel over gemcitabine or polysorbate-based docetaxel in experimental pancreatic cancer. Carcinogenesis *34*, 2361-2369.

Brown, S.A., Fleury-Olela, F., Nagoshi, E., Hauser, C., Juge, C., Meier, C.A., Chicheportiche, R., Dayer, J.M., Albrecht, U., and Schibler, U. (2005). The period length of fibroblast circadian gene expression varies widely among human individuals. PLoS Biol *3*, e338.

Cerami, E., Gao, J., Dogrusoz, U., Gross, B.E., Sumer, S.O., Aksoy, B.A., Jacobsen, A., Byrne, C.J., Heuer, M.L., Larsson, E.*, et al.* (2012). The cBio cancer genomics portal: an open platform for exploring multidimensional cancer genomics data. Cancer Discov *2*, 401-404.

Ellenrieder, V., Hendler, S.F., Boeck, W., Seufferlein, T., Menke, A., Ruhland, C., Adler, G., and Gress, T.M. (2001). Transforming growth factor beta1 treatment leads to an epithelial-mesenchymal transdifferentiation of pancreatic cancer cells requiring extracellular signal-regulated kinase 2 activation. Cancer Res *61*, 4222-4228.

Gao, J., Aksoy, B.A., Dogrusoz, U., Dresdner, G., Gross, B., Sumer, S.O., Sun, Y., Jacobsen, A., Sinha, R., Larsson, E.*, et al.* (2013). Integrative analysis of complex cancer genomics and clinical profiles using the cBioPortal. Science signaling *6*, pl1.

Lieber, M., Mazzetta, J., Nelson-Rees, W., Kaplan, M., and Todaro, G. (1975). Establishment of a continuous tumor-cell line (panc-1) from a human carcinoma of the exocrine pancreas. Int J Cancer *15*, 741-747.

Livak, K.J., and Schmittgen, T.D. (2001). Analysis of relative gene expression data using real-time quantitative PCR and the 2(-Delta Delta C(T)) Method. Methods *25*, 402-408.

Sporl, F., Schellenberg, K., Blatt, T., Wenck, H., Wittern, K.P., Schrader, A., and Kramer, A. (2011). A circadian clock in HaCaT keratinocytes. J Invest Dermatol *131*, 338-348.

Watanabe, M., Sheriff, S., Lewis, K.B., Cho, J., Tinch, S.L., Balasubramaniam, A., and Kennedy, M.A. (2012). Metabolic Profiling Comparison of Human Pancreatic Ductal Epithelial Cells and Three Pancreatic Cancer Cell Lines using NMR Based Metabonomics. J Mol Biomark Diagn *3*, S3-002.